UNIVERSITY OF TARTU
Faculty of Science and Technology
Institute of Physics

Siim Heinsalu

Plasmon-enhanced fluorescence in TiO2:Sm^{3+} films co-doped with gilded silica nanoparticles

Bachelor's thesis

Supervisors: PhD Leonid Dolgov
PhD Ilmo Sildos

Tartu 2014

Contents

List of symbols

n	– refractive index
μ	– permeability
ε	– dielectric permittivity
x	– displacement of the electron
m_e	– effective mass of the electron
γ	– frequency of collisions for the electrons with ionic lattice
q	– charge of the electron
E	– electric field strength
n_e	– volume density of the electrons
ω_p	– plasma frequency
P	– dipole polarization of material
ω	– frequency of the external electric field
i	– imaginary unit
t	– time
D	– dielectric displacement
ε'	– real part of dielectric permittivity
ε''	– imaginary part of dielectric permittivity
ε_0	– dielectric constant of vacuum
ε_d	– permittivity of neighbouring dielectric
E_0	– electric strength of incident light
E_{dep}	– electric strength of the depolarization field
E_L	– resultant local electric field
dE_{dep}	– differential element of depolarization of the electric strength
r	– radius of the particle
S	– surface area
dS	– unit surface area
χ	– dielectric susceptibility
λ	– wavelength of incident light
α	– polarizability of the particle
N_p	– number of dipoles
ΔV	– volume of a nanoparticle
M	– molar mass

N_a – Avogadro constant

ρ – density of the particles

σ_{sca} – scattering cross section of the nanoparticle

I – intensity of light

I_o – initial intensity of light

C – speed of light

$\Delta\Omega$ – element of solid angle

E_r – horizontal component of the electric strength

E_l – vertical component of the electric strength

k – wave number

I_r – intensity of light scattered in horizontal direction

I_l – intensity of light scattered in vertical direction

λ_0 – wavelength of light in vacuum

n_{med} – refractive index of medium

l – order of dipole

x_s – size parameter

P_l – Legendre polynomial

m – complex refractive index of the nanoparticle

m – real part refractive index of the nanoparticle

m – imaginary part refractive index of the nanoparticle

k – imaginary part of refractive index

$\psi_l(x)$ – spherical Bessel function of first kind

$\chi_l(x)$ – spherical Bessel function of second kind.

$\xi_l(x)$ – Ricatti-Bessel function

$D_n(x)$ – derivative of Spherical Bessel function

$a_n \& b_n$ – Mie coefficients

σ_{Ver} – part of the cross section corresponding to the light scattered in vertical plane

σ_{Hor} – part of the cross section corresponding to the light scattered in horizontal plane

τ_n – angular dependent function expressed in Legendre polynomials

π_n – other angular dependent function expressed in Legendre polynomials

$J_l(x)$ – Bessel function of the first kind

$Y_l(x)$ – Bessel function of the second kind

η – quantum yield

σ_{eff} – absorption cross section

Γ_{rad} – radiative decay rate

Γ_{nonrad} – nonradiative decay rate

τ – lifetime of fluorescence emission

σ_{abs}^{eff} – effective absorption crosssection

Γ_{ET} – rate of energy transfer

Γ_{nonrad}^{o} – nonradiative decay rate without energy transfer

F – quantum yield of total fluorescence

λ_{ex} – excitation wavelength

λ_{em} – emission wavelength

$\vec{E}^0$ – electric strength of local field

$\vec{E}$ – electric strength of local field near the metal

$\vec{p}$ – molecular dipole moment

$f(\lambda')$ – integral of normalized fluorescence spectrum

α_{abs} – absorption coefficient

ρ – concentration of particles dispersed in the liquid

L – optical path length

A – light absorption for water dispersion of metal nanoparticles

$\langle\tau\rangle$ – average fluorescence lifetime

1. Introduction

1.1. Relevance of plasmonics as a path to nanooptics

Long before the beginning of the metal optic science artists used small noble metal particles in the creation of such artefacts as coloured glass tableware and stained glass windows. One of the famous examples is the Lycurgus cup [1] which has a dull green appearance while reflecting light and turns red when illuminated by transmitted light. The metal nanoparticles inside the glass are about 70 nm in size. So it would be impossible to see them with the naked eye or even by an optical microscope.

One of the earliest investigations of colours inherent to the dispersions of metal nanoparticles was done by M. Faraday. He prepared reproducible and stable water dispersions of gold nanoparticles and described their properties. M. Faraday also used prepared gold colloids for lecture demonstrations. Now they are exhibited in the M. Faraday museum at the Royal Institution of Great Britain [2].

Subsequent investigations for optical properties of nanostructured metals were intensified since the beginning of R. Wood works. He discovered the unusual narrow asymmetric absorption lines in the spectra of light reflected from the metal diffraction gratings. These lines were named as Wood's anomalies [3].

Theoretical background explaining the coloration of nanoparticles' dispersions was further developed by Gustav Mie [4]. Current scientific and applied interest is directed to the local manipulation with light in terms of its spectral distribution, directionality, intensity in the vicinity of metal nanoparticles. They allow guiding of light energy at scales smaller than diffraction limit. The guiding can be done with nanostructuring of optical components and joining them with electronic elements as nano-waveguides in the integrated chips [5]. At first sight using metal nanoparticles for the guidance of light energy seems problematic, due to high optical losses in metals. An elegant solution to this problem is connected with using of light induced surface plasmons as collective oscillations of surface electrons in metal nanoparticles. Resonance coupling of light and plasmons results in confinement of the energy near the surface of nanostructured metal. It occurs below the diffraction limit for the light waves and energy can be transferred in the nanolayer on the distances up to several tens of microns [6]. Since surface plasmons work at optical frequencies this could guarantee saving of high rates in data interchanges for future nanoscale opto-electronic chips and faster computers if the energy losses aren't be big.

Doping of composite systems by noble metal nanoparticles can be used for the improvement of their optical behaviour. For instance: placing metal nanoparticles near fluorescent molecules would gain fluorescence. This effect is caused by supporting of light waves with surface plasma electronic oscillations in the metal nanoparticles [7, 8].

In the present thesis the investigation of fluorescence enhancement in the visible spectral range caused by metal nanoparticles is carried out for the sol-gel metal oxide films activated with fluorescent rare earth ions. Previous investigations of sol-gel systems with noble metal nanoparticles mainly have been devoted to the plasmonic influence on the non-linear processes [9] or enhancement of near-infrared fluorescence [10]. So this investigation is quite novel.

1.2. Structure of the work and author contribution

The text is structured in the following way. Section 1.1 describes relevance of the topic and contains the survey of literature representing the state of the art in field of plasmonics. Section 2 is about materials and methods used in this work for the experimental realization of plasmon enhanced fluorescence. Section 3 contains theoretical review background containing concepts, which will be used and developed in explanation of experimental results. Particularly paragraph 3.1 is devoted to the principles of Drude theory and description of light induced polarization and negative permittivity for the metals in the optical spectral range. It was concluded that in addition to positive permittivity of environment to concept of negative permittivity for noble metals is introduced, which is a basis for surface plasmon resonance. Resonance interaction of light with surface electrons causes locally strong electric fields on the metal-dielectric interface. It causes resonant increase in the amplitudes of light in the induced electric field, light scattering and light absorption, which are described in the paragraphs 3.2 and 3.3. Paragraphs 4.1 and 4.2 describe prerequisites for using resonant behaviour of metal permittivity for the coupling of surface electronic oscillations in the metal nanoparticle with absorbed or emitted light by fluorophore. Section 5 contains our original results of application of the Mie theory for determination of particles sizes and their concentration in colloid. It also contains results of dark field microscopy and rare earth plasmon enhanced fluorescence with their discussion. Conclusions are formulated in section 6. All experimental results described in the thesis were obtained by Siim Heinsalu in collaboration with scientists from the Laboratory of laser spectroscopy at the Institute of Physics, University of Tartu. Siim Heinsalu took part in scientific discussions and the preparation of reports and publications. Siim Heinsalu presented the results at 2 international scientific conferences and 1 international summer school. The results are published in the Nanoscale Research Letters journal, Springer [11].

2. Materials and methods

The samples investigated in the present work are TiO_2 films activated by the Sm^{3+} fluorescent ions and doped with gilded nanoparticles. Sm^{3+} rare earth fluorophore was chosen because of its photostability and spectral coincidence of its fluorescence with plasmonic resonance band of gilded nanoparticles dispersed in the TiO_2 host. Preparation of TiO_2 host and gilded nanoparticles is described in sequence. It is also pointed out at which stage the rare earth salt, as a source of fluorescent ions, was added to the precursor.

Sol-gel method was used in this work for the preparation of TiO_2 films. It is a prospective approach for the inexpensive preparation of optical quality samples shaped both as volume pieces as well as thin films and fibers [12]. The process starts from the precursor consisting of the metal-organic molecules in which the atom of the metal is connected to the alkoxide group.

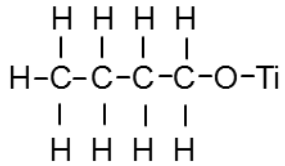

Fig. 1. Titanium *n*-butoxide.

As an example, titanium butoxide is presented in Fig. 1. Addition of certain amount of water to such molecules causes their hydrolysis with the release of initial alcohol and formation of TiO_2 gel through the polycondensation of unstable titanium hydroxide molecules into 3D [-Ti-O-Ti–] network (Fig. 2).

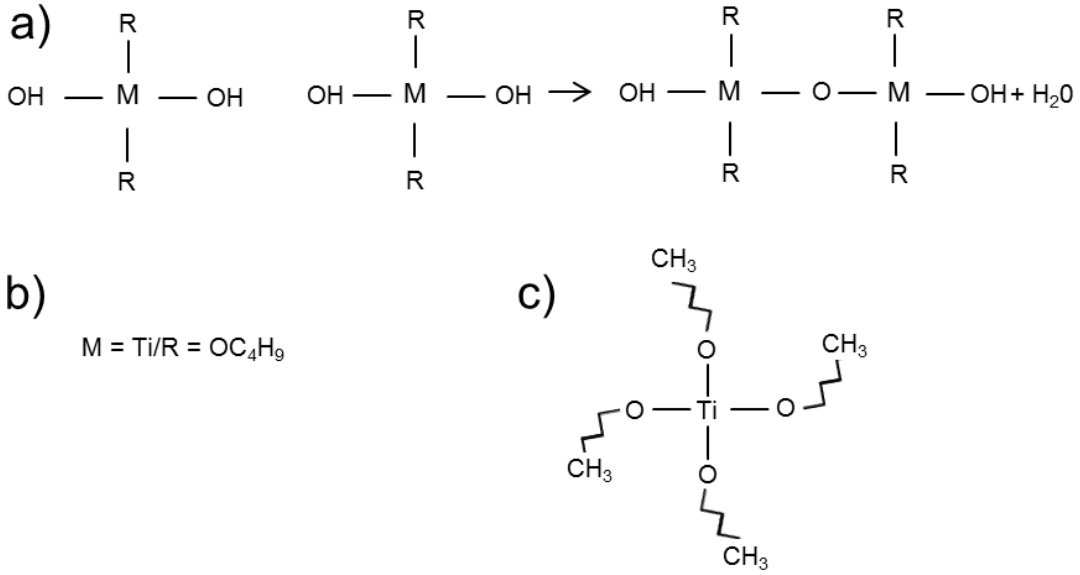

Fig. 2. (a) Scheme of $TiOC_4H_9$ hydrolysis and formation of Ti-O-Ti network, (b) notation conventions, (c) titanium butoxide stoichiometry from ref [13].

The polycondensation process would then be continued with the creation of larger and larger molecules by means of polymerization, when dimers, trimers and higher orders of -mers are joined into polymer chains [13]. Initially the nuclea of gelation with size of several angstroms appear. They are so small that gravitational forces for them are negligible compared to the short-range van der Waals forces [14]. Then bigger molecules are formed in the process of growth. They would have at least two bonds for connection with other monomers. Finally, gelled material is obtained. Gelled materials consist of fragments that have microscopic size. They also intensively scatter light therefore quick transition from the sol to gel states can be recognized by the material turbidity.

To prevent undesirably quick gelation there are many possibilities. One of them is just slow down gelation by intensive stirring. Another way is the additions of special compounds, which act as scavengers for free bonds responsible for polycondensation.

Different kinds of materials can be prepared by sol-gel method (Fig. 3). The appearance of resulting material depends on the velocity of gelation and evaporation of the solvent. Quick evaporation of solvent results in formation of dense xerogel, which can give continuous coating after annealing (Fig. 3, stages 11, 13). TiO_2 films, which are undoped and doped by gold nanoparticles and activated by Sm^{3+} ions were formed by means of spincoating of sol solution in *n*-butanol with addition of small amount of water. Further gelation and annealing at 500°C during 1 hour results in the formation of solid TiO_2 films on the glass substrates. The thickness of obtained films was in the range of 150-200 nm determined by spectral measurements of light interference.

Termination of the gelation process at certain stage, caused by the finishing of the reacting components or by addition of scavenger compounds, results in the formation of separate nanoparticles (Fig. 3, stage 14). Our silica nanoparticles were formed on the basis of such reaction by the modified Stöber method [15]. Continuous mixing of the precursor allows to obtain uniform growth of the nanoparticles in whole the volume of the solution. The scanning electron microscopy proved formation of uniform silica nanoparticles with average size in the range of 160-200 nm (Fig. 4).

At the end we briefly describe principles of preparation for different kinds of sol-gel materials, which were not used in the present work, but which could be applied in our further investigations. Decrease of water content in combination with slow evaporation of solvent results in a viscous precursor suitable for obtaining sol-gel fibers (Fig. 3, stages 7-14). Very slow evaporation of solvent results in the formation of porous ceramics.

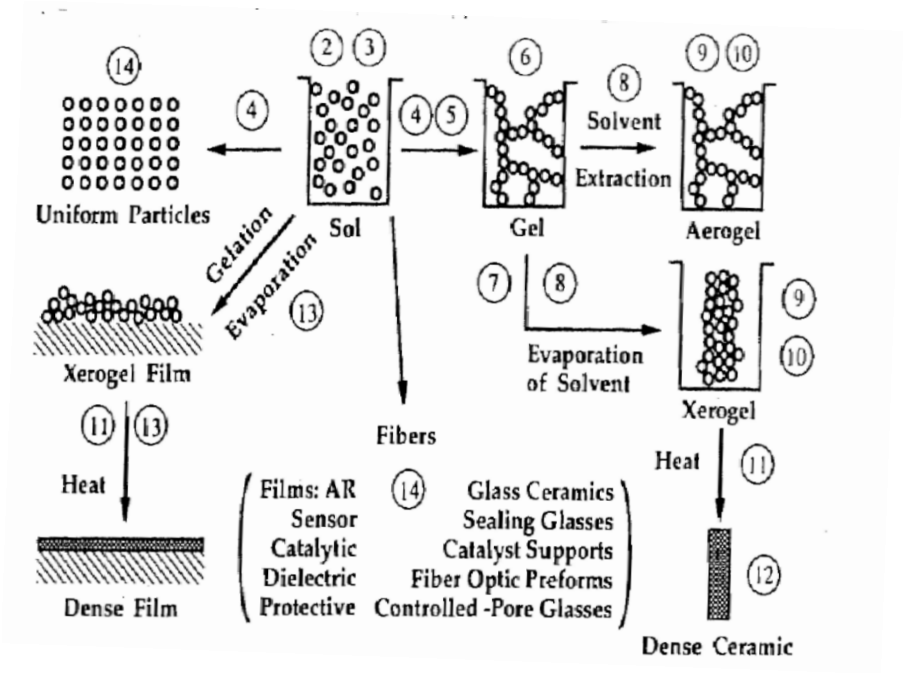

Fig 3. Simplified representation of the different phases or routes for sol-gel technology [13].

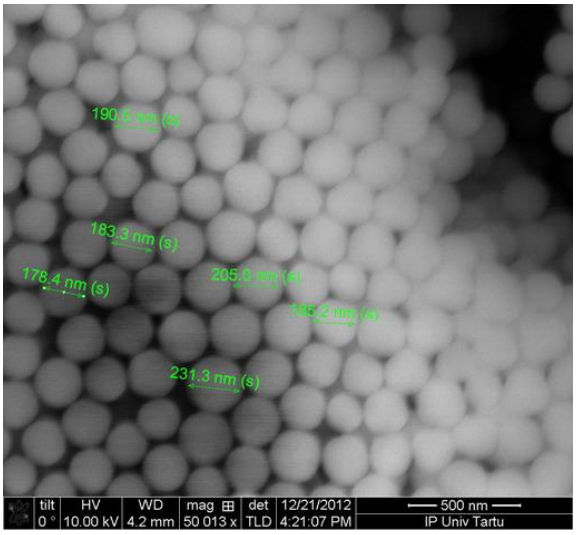

Fig. 4. Scanning electron microscopy image of silica nanoparticles before covering with the gold shell of our result.

Now let's turn to the preparation of gilded nanoparticles. The preparation of big enough monodispersed spherical metal nanoparticles is quite a complicated task. Therefore, first we prepared the monodispersed silica cores and then covered them by the gold shell by the method described in Ref [16]. Following description of optical properties for such nanoparticles dispersed in water and in the TiO_2 host testifies that in case of a comparatively thick ~ 20 nm gold shell they behave similarly to the continuous metallic particles of equivalent size. It is confirmed also by literary data [17]. Such nanoparticles have received quite a lot of notice because of the ability to be

reproduced without any big difficulties and due to their stability [18]. Silica cores were specially modified by the amino groups for the better adsorption of the gold seeds (Fig. 5) on their surface. Gold seeds were obtained from the water solution of hydrochloroauric acid. At the final stage of synthesis the gold seeds were precipitated on the surface of silica cores and connected together for the formation of continuous gold shells around the silica cores.

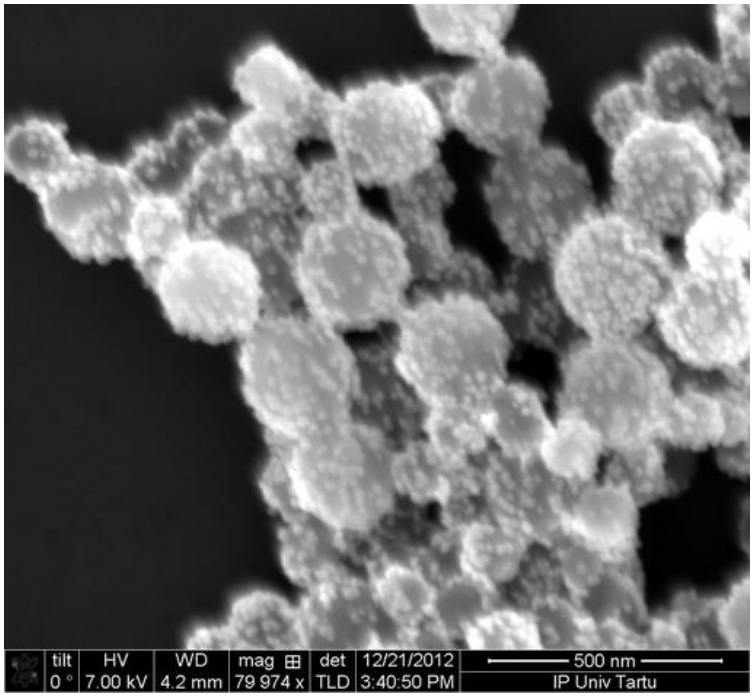

Fig. 5. Scanning electron microscopy image of silica nanoparticles with partially formed gold shells on their surface of our result.

Core-shell silica-gold nanoparticles and samarium salt serving as a source of fluorescent Sm^{3+} ions were added and ultrasonically mixed with the titanium butoxide sol precursor before the stage of film deposition. Such addition of the dopants in the pre-final stage of films preparation allows preparation of not only neat referent TiO_2 coatings and TiO_2 coatings activated by Sm^{3+} fluorescent ions, but also coatings containing gilded nanoparticles in addition to the already mentioned components.

Using gilded nanoparticles in our experiments has some additional advantages. First would be that gilded nanoparticles in our case have the same optical properties as purely metal nanoparticles. But the main advantage when compared to pure metallic nanoparticles is that we can configure the absorbance or plasmon resonance between visible and infrared range in the spectrum by changing the silica core thickness [16]. Lastly, the spherical configuration is quite easily made and maintained compared to pure metal nanoparticles.

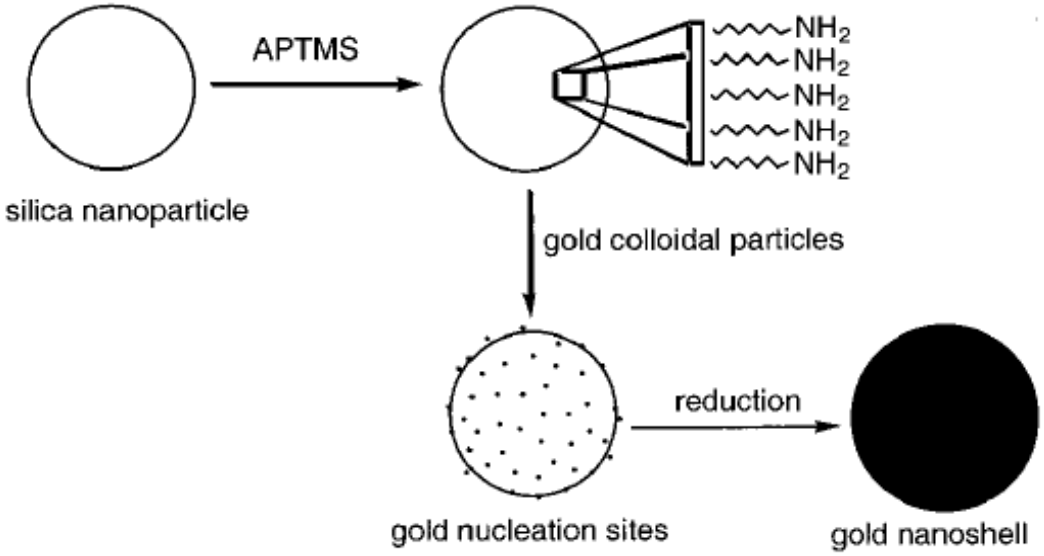

Fig 6. The scheme of growing gilded nanoparticles from the Ref [16].

The optical imaging and microluminescence measurements were carried out in a home-assembled setup based on the Olympus BX41M microscope (Olympus Corporation, Shinjukuku, Japan), combined with a Andor iXon electron-multiplying charge-coupled (EMCCD) camera device (Springvale Business Park, Belfast, UK) for highly sensitive optical imaging and fiber-coupled Andor SR303i spectrometer with a Andor Newton camera for spectral measurements. A coloured image of light scattering of a bigger sample area was made with a digital photocamera attached to an ocular of the microscope because the EMCCD camera used for fluorescence imaging has only a black and white mode. Both dark field and fluorescence measurements were carried out by using a side illumination. In the case of dark field imaging, the beam of a bright white light emitting diode (LED) was used so that the field of view remains dark if no scattering entities were present in the sample. The fluorescence was excited with a 355 nm diode-pumped solid-state (DPSS) laser while the signal was observed though a long-pass filter. In the latter case, the small aperture of the single-mode fiber allowed highly confocal spectral measurements in spite of the wide-field illumination. Alternatively, spectral measurements with point excitation were possible by using 532 nm DPSS laser focused onto the sample through the microscope objective. Fluorescent lifetimes were measured by a multichannel analyzer P7882 (FAST ComTec, München, Germany) connected to the photomultiplier.

3. Theoretical background of light scattering by metal colloids

3.1. *Interaction of light with metal in the approximation of Drude model*

3.1.1. Concept of negative permittivity of metals

Here we shall review introduce the concept of negative permittivity for the metals in the optical spectral range and demonstrate how negative permittivity of the metal causes the local resonant increase in electric field near the metal nanoparticle [19-21].

Light can be represented as a wave of electromagnetic energy. Let's estimate the role of electric and magnetic vectors of light in the optical phenomena. Magnetic permeability of most materials used in optics is close to 1. Therefore magnetic contribution into refractive index *n* is very small: $n = \sqrt{\varepsilon\mu}$, but if μ=1, then the refractive index depends only on the dielectric permittivity $n = \sqrt{\varepsilon}$. Dielectric permittivity of the material depends on the light-induced polarization [19], which is caused by the electric component of light. Light-induced polarization in metals can be approximately considered as a displacement of free electrons or electronic plasma surrounding the ionic lattice. The term "plasmonics" originates from such classical consideration firstly proposed by P. Drude [20].

The Drude model represents a metal as a lattice of positively charged ions immersed into plasma consisting of free electrons. Of course it is quite a rough model, because currently the quantum mechanical model of metals is accepted as more accurate [21]. But Drude theory is a suitable approach for our purpose to describe the ideas of plasma frequency and negative permittivity of metals. Historical and modern significance of this theory is due to by its valid applications for the explanation of the E. Hall effect, specific conductivity of metals in direct and alternate currents and thermal conductivity.

Metal is electrically neutral at normal conditions. However, there could be some local areas where electrons are shifted from the ions because of electronic density fluctuations. It causes electric charge which is not compensated. Electric force acting on the one electron tends to return it to its initial position, but because of momentum conservation the electron continues its oscillation. In differential form this is equal to a differential equation of second order in displacement *x* of electron:

$$m_e\ddot{x} + m_e\gamma x = -qE, \qquad (1)$$

where m_e is the effective mass of the electron, γ – the frequency of collisions of the electrons with ionic lattice, q – charge of the electron, E – the electric field strength. Taking into account Gauss's theorem as a relation between the electric field induced in metal layer and its charge.

$$E = \frac{n_e q x}{\varepsilon_0}, \tag{2}$$

where n_e is the volume density of the electrons and ε_0 the vacuum permittivity, we can substitute (2) to (1) which changes our differential equation to:

$$m_e \ddot{x} + m_e \gamma x = -\frac{n_e q^2 x}{\varepsilon_0}, \tag{3}$$

$$m_e \ddot{x} + m_e \gamma x + \frac{q^2 n_e x}{\varepsilon_0} = 0, \tag{4}$$

$$\ddot{x} + \gamma x + \frac{q^2 n_e}{m_e \varepsilon_0} x = 0. \tag{5}$$

The coefficient near the x variable in this equation can be defined as the square of plasma frequency:

$$\frac{q^2 n_e}{m_e \varepsilon_0} = \omega_p^2. \tag{6}$$

This is the frequency of free oscillations of the volume electronic plasma. This frequency is also proportional to the square root of the concentration of electrons n_e, the charge of electron q and inversely proportional to its effective electron mass.

All metals are initially identical when it comes to plasma frequency, because they have the same values specified in (6) in the Drude approximation, but real metals differ due to their colour, electric conductivity and thermal conductivity. This is because the concept of free electrons can be strictly applied only for a small class of alkaline metals truly having similar properties. However, other metals have partially bounded electrons, which can differently influence on plasma frequency. Therefore, for real metals we need to use additional corrections to the Drude theory.

Plasma frequency is an important value for the metal, because it defines the metal permittivity and consequently refractive index and optical properties. Let's consider dipole polarization P of the metal in order to demonstrate the relationship between the permittivity of metal and its plasma frequency:

$$P = -n_e q x, \tag{7}$$

where x is the solution for the equation (5).

The solution can be represented in complex form:

$$x(t) = \frac{q}{m_e(\omega^2 + i\gamma\omega)} E(t), \tag{8}$$

where ω – frequency of the external electric field, i is imaginary unit and t is time.

Substituting this equation (8) into (7) we shall obtain:

$$P = -\frac{n_e q^2}{m_e(\omega^2 + i\gamma\omega)} E, \tag{9}$$

Substitution of (9) into the equation (10) for the dielectric displacement:

$$D = \varepsilon_0 E + P, \tag{10}$$

will give us:

$$D = \varepsilon_0 (1 - \frac{\omega_p^2}{\omega^2 + i\gamma\omega}) E. \tag{11}$$

This contains the dielectric permittivity of free electron gas as the following factor:

$$\varepsilon(\omega) = 1 - \frac{\omega_p^2}{\omega^2 + i\gamma\omega}. \tag{12}$$

One can see that in the case of a small damping γ and in the frequency range $\omega << \omega_p$ the real part of dielectric permittivity ε' can be negative:

$$\varepsilon'(\omega) = 1 - \frac{\omega_p^2}{\omega^2}. \tag{13}$$

3.1.2. Localization of electric field near metal nanoparticle

Possibility of negative value makes the permittivity in alternating electric field different from the usually positive value of static permittivity. The negative value of the permittivity makes it possible to have a resonance between the electric field of light wave and surface oscillations of the electronic plasma in the metal. Further we demonstrate that such resonance causes strong local enhancement of electric field in the vicinity of the metal nanoparticle, which plays an important role in light absorption and light scattering by metal nanoparticles.

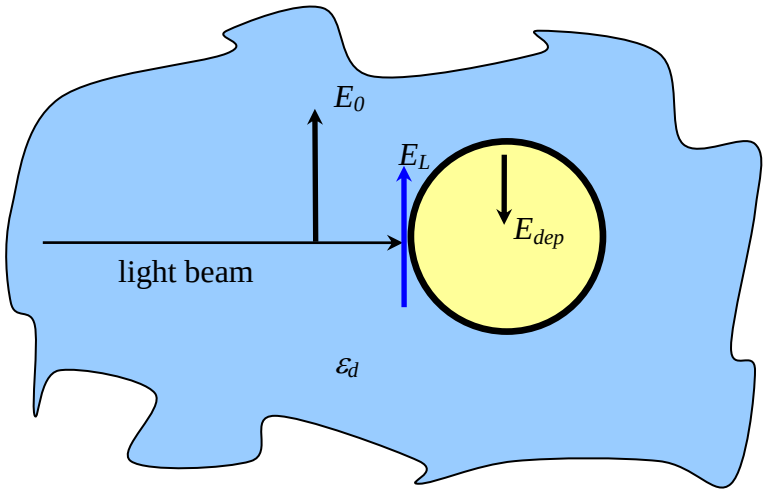

Fig. 7. Scheme of electric fields acting on the metal nanoparticle: E_0 – electric field of incident light, E_{dep} – depolarization field, E_L – resultant local electric field, ε_d – permittivity of neighbouring dielectric.

Here we assume that the metal particle is small in comparison with the wavelength of light. Changes of the light electric strength in the vicinity of the particle are also so small, that we can consider electric strength as a static value at a certain moment. It is so-called electrostatic approximation, which looks a little synthetic, because we suppose the field to be static, but say that permittivity could be negative. However such approach is appropriate for the illustration of locally enhanced electric strength and applied in the Refs [9, 22].

Resultant local electric field E_L acting on the particle will consist of the incident electric field E_0 and the depolarization field E_{dep} caused by the polarization of nanoparticle atoms. If particle is situated in the medium with permittivity ε_d, the equation for the local field is:

$$E_L = \frac{E_0}{\varepsilon_d} + E_{dep}. \qquad (14)$$

The differential element of depolarization of the electric strength dE_{dep} can be represented according to the Gauss's theorem by the sum of charges enveloped by the element dS of nanoparticle's surface:

$$dE_{dep} = \frac{P\cos(\theta)dS}{4\pi\varepsilon_0 r^2}, \qquad (15)$$

where θ stands for angle between the normal to the unit surface area dS and the polarization direction P and r is the radius of the particle.

$$E_{dep} = \int_0^{\pi} \frac{P\cos^2(\theta)}{4\pi\varepsilon_0 r^2} 2\pi r^2 \sin(\theta)d\theta = \frac{P}{3\varepsilon_0}. \qquad (16)$$

We shall set a minus sign before the value obtained in equation (16). It is because the depolarization field is directed oppositely to the incident field, so for the resultant local field:

$$E_L = \frac{E_0}{\varepsilon_d} - \frac{P}{3\varepsilon_0}. \quad (17)$$

Polarization P of particle can be represented by the use of the electric susceptibility χ:

$$P = \varepsilon_0 \chi E_L, \quad (18)$$

where

$$\chi = \frac{\varepsilon'}{\varepsilon_d} - 1. \quad (19)$$

And ε' is the real part of particle permittivity Substitution of (19) and (18) into (17) finally resulted in:

$$E_L = \frac{3}{2\varepsilon_d + \varepsilon'} E_0. \quad (20)$$

One can see that the denominator of this fraction is close to zero, when

$$\varepsilon' = -2\varepsilon_d. \quad (21)$$

Such a resonance condition causes stronger enhancement of the local electric field E_L near the particle. It will be shown that the same resonance denominator is presented in the equations for the light absorption and light scattering cross sections of metal nanoparticles. It stipulates stronger resonance absorption and scattering of light by metal nanoparticles at the spectral range of plasmonic resonance. These phenomena are considered in the next paragraph.

3.2. Plasmonic resonance in case of Rayleigh' light scattering

In this paragraph we shall consider resonant scattering of light by the light-induced dipole, which can be considered as a model of a small enough metal nanoparticle, which has the size not more than λ/20 [7].

Light scattering can be understood as a change in direction of light propagation, when light meets the nanoparticle. The electric field of incident light causes changes in electric polarization of nanoparticle. Moving electric charges inside the nanoparticle are the sources of secondary electromagnetic waves. Scattered light can be imagined as a result of interference of these secondary waves [23]. Let's consider the case of a small particle with a size which is not bigger than λ/20, where λ is the wavelength of incident light. It corresponds to the static approximation considered in the paragraph 3.1.2.

Using the concept of the local electric field introduced in the equation (14) we can write down [24] the polarization P of the unit volume of nanoparticle material with the polarizability α of the metal atoms, N_p number of these atoms and ΔV a volume of metal nanoparticle, E_L local field as:

$$P = \frac{N_p}{\Delta V}\alpha E_L . \tag{22}$$

It is also possible to represent polarizability α of the metal atom in Clausius-Mossotti view by derivation of localized electric field E_L through the permittivity of metal ε. This will give us [24,25]

$$\alpha = \frac{3M}{N_a \rho}\frac{\varepsilon - 1}{\varepsilon + 2} = \frac{3}{4\pi}\frac{\varepsilon - 1}{\varepsilon + 2}\frac{\Delta V}{N_p}, \tag{23}$$

where M is the molar mass, N_a the Avogadro constant, ρ density of particles.

The energy scattered by the nanoparticle to the element of surrounding spherical surface in unit time is $Ir^2 \sin(\theta) d\theta d\gamma$ (Fig. 8). To obtain energy passing through the whole sphere in unit time we need to make the integration over the polar angle and azimuthal angle [26]. This integration will give us part of the energy which is scattered by nanoparticle. Since we need to compare this scattered energy with the whole incident energy we introduce the scattering cross section σ_{sca}, which illustrates what part of the energy is scattered by one nanoparticle:

$$\sigma_{sca} = \frac{1}{I_0}\int_0^{2\pi}\int_0^{\pi} Ir^2 \sin(\theta) d\theta d\gamma , \tag{24}$$

where I is the intensity of scattered light and I_o the intensity of incident light.

Under the integral we have the intensity of light scattered by dipole. To clarify the value of this intensity we shall use Poynting equation, which connects the light intensity with the electric field strength

$$I = \frac{1}{\Delta\Omega}\frac{c}{4\pi}\left|\vec{E}\right|^2 , \tag{25}$$

where c is the speed of light and $\Delta\Omega$ the element of solid angle. The electric strengths of the scattered field can be divided on the horizontal $\left(\gamma_1 = \frac{\pi}{2}\right)$ and vertical $\left(\gamma_2 = \frac{\pi}{2} - \theta\right)$ angle components (Fig. 8). For these components we shall have [25]:

$$E_r = -E_{or}\frac{\exp\left(-ik\left(r - ct\right)\right)}{r}k^2 \alpha \sin(\gamma_1), \tag{26}$$

$$E_l = -E_{ol}\frac{\exp\left(-ik\left(r-ct\right)\right)}{r}k^2\alpha\sin\left(\gamma_2\right). \tag{27}$$

Where $k=\frac{2\pi}{\lambda}$ is the wavenumber in vacuum and in a medium it would be multiplied with its refractive index n_{med}. Substitution of (26) & (27) into (25) will give horizontal and vertical components of light intensities:

$$I_r = I_{0r}k^4\frac{\alpha^2}{r^2}, \tag{28}$$

$$I_l = I_{0r}k^4\frac{\alpha^2}{r^2}\cos\left(\theta\right)^2. \tag{29}$$

Finally the summation of the vertical and horizontal components of light intensity will give us the light intensity of Rayleigh scattering.

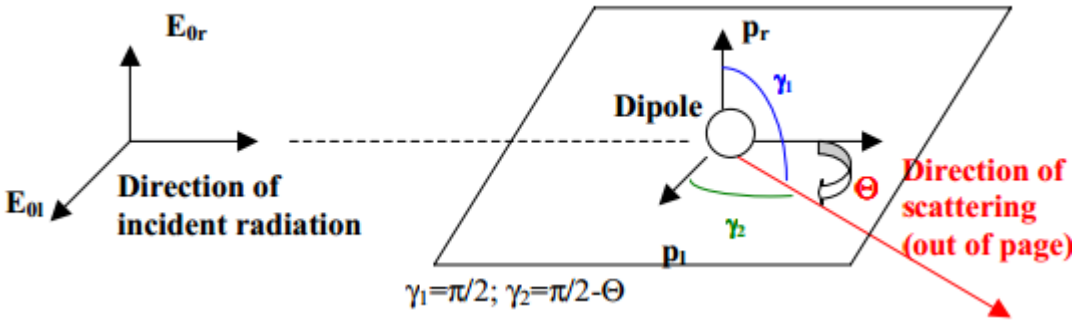

Fig. 8. Schematic position of dipole, which scatters light with relative geometrical notation [26].

Since we started from a dipole moment we should look at how the intensity itself can be written down by means of oscillating dipole moment:

$$I = \frac{\left(1+\cos\left(\theta\right)^2\right)k^4\alpha^2}{2r^2}I_0. \tag{30}$$

From the substitution of the equation (23) to (30) and expressing the wave number through the wavelength we obtain

$$I = \frac{I_0}{r^2}\frac{\left(1+\cos\left(\theta\right)^2\right)}{2}\left(\frac{2\pi}{\lambda}\right)^4\left(\frac{3}{4\pi}\frac{\varepsilon-1}{\varepsilon+2}\frac{\Delta V}{N_p}\right)^2. \tag{31}$$

And now by substituting (31) into (24) we have

$$\sigma_{sca} = \frac{128\pi^5r^6}{3\lambda^4}\left|\frac{\varepsilon-1}{\varepsilon+2}\right|^2. \tag{32}$$

The scattering cross section obtained in the equation (32) becomes high if ε is close to -2, which corresponds to the similar resonance behaviour of local electric field in the equation (20).

3.3. Mie model of light scattering

Analysis of the light scattering intensity (31) and cross section (32) gives an imaginary impression that the shape and spectral position of the plasmonic resonance does not depend on the particle radius *r*. Experimental spectra of the light scattering obtained by us and other authors, for example Ref. [27], testify about the red-shift and broadening of the resonance band width increase of the particle size. These effects cannot be explained by the Rayleigh theory. The necessary extension to the Rayleigh theory gives Mie approach to the light scattering. Mie theory represents more general approach not only to the light scattering, but also to the light absorption by small particles.

Rayleigh model describes the particular case of light scattering, when the size of the scattering nanoparticles is less than the wavelength of incident light. Light scattering by the particles with sizes comparable with the wavelength of light is described by the more general Mie theory. In addition to the light-induced dipole polarization, which is well described earlier by Rayleigh model, quadrupole, hexapole, octupole and other higher orders of multipoles are induced in the bigger nanoparticles (Fig. 9). Mie theory is devoted to the calculation of the light extinction as a summarized impact from several multipoles. In contrast to the Rayleigh model which considers only the electric dipole, the Mie model can consider electric multipoles of higher order. The multipoles are then added together and expressed by Mie coefficients a_l and b_l, where *l*= 1 is for dipole, *l*=2 is for quadrupole, *l*=3 hexapole and so on.

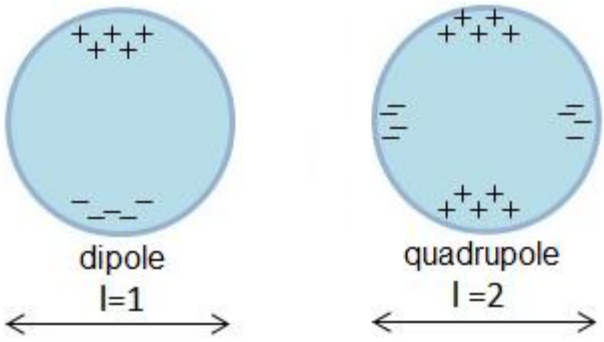

Fig. 9. Scheme of dipole and quadrupole polarisation in metal particle.

Mie theory was developed in 1908, but it is still in active use and undergoing modernization. In the recent years several implementations of the Mie light scattering solutions have been made in different computer languages [28, 29]. These implementations allow calculation not only light scattering, but also the scattering phase function and the light extinction. Additionally the Mie model was generalized also for the particles with more complex shapes, such as cylinders [30], particles with complex shapes [31, 32] . The Rayleigh theory is applicable for the particles for which the radius *r* is:

$$r << \frac{\lambda_0}{2\pi n_{med}|m|}, \tag{33}$$

where λ_0 is the wavelength of light in the vacuum, n_{med} the refractive index of medium and m the complex refractive index of a particle.

The Mie theory is applicable both for the values of r appropriate for the Rayleigh theory and for the higher particle sizes comparable with the wavelength of light [7].

The intensity of scattered light calculated in the frame of the Mie model can be also represented as a sum of intensities connected with vertical and horizontal projections of the electric strength vector (Fig. 8 in paragraph 3.2). Moreover, since those intensities are proportional to the cross sections we have for differential cross section:

$$\sigma_{sca} = \sigma_{Hor} + \sigma_{Ver} = \frac{\lambda^2}{8\pi^2}(i_1 + i_2). \tag{34}$$

Here σ_{Ver} & σ_{Hor} are cross sections corresponding to the light scattered in horizontal and vertical planes and i_1 & i_2 are angular scattering intensity functions for the both horizontal and vertical components.

The intensity functions itself are calculated in terms of infinite series in form of [33]:

$$i_1 = \left|\sum_{l=1}^{\infty} \frac{2l+1}{l(l+1)}\left[a_l \pi_l(\cos(\theta)) + b_l \tau_l(\cos(\theta))\right]\right|^2, \tag{35}$$

$$i_2 = \left|\sum_{l=1}^{\infty} \frac{2l+1}{l(l+1)}\left[a_l \tau_l(\cos(\theta)) + b_l \pi_l(\cos(\theta))\right]\right|^2. \tag{36}$$

Where l is the order of the multipole, a_l and b_l Mie coefficients, τ_l and π_l are angular dependent functions expressed in Legendre polynomials.

However, since the dipole order can't extend to the infinity in our calculations, the highest value for the electric dipole order x should be handled by the equation [34]:

$$l_{\max} = \left[x_e + 4x_e^{1/3} + 2\right], \tag{37}$$

where $x_e = \frac{2\pi r n_{med}}{\lambda_0}$ is the size parameter.

Angular dependent functions $\tau_n(\cos(\theta))$ & $\pi_n(\cos(\theta))$ are expressed by Legendre polynomials:

$$\tau_n(\cos(\theta)) = \frac{dP_n(\cos(\theta))}{d\theta}, \tag{38}$$

$$\pi_n(\cos(\theta)) = \frac{P_n(\cos(\theta))}{\sin(\theta)}. \tag{39}$$

The Legendre polynomials of the first order are expressed as:

$$P_l(x) = \frac{1}{2^l\, l!}\frac{d^l}{dx^l}\left[\left(x^2-1\right)^l\right]. \tag{40}$$

Thus by plugging Eq. (35)-(40) into (34) one would derive such an equation:

$$\sigma_{sca} = \frac{2}{K^2}\sum_{l=0}^{\infty}(2l+1)\left(|a_n|^2 + |b_n|^2\right). \tag{41}$$

Where a_n and b_n are the Mie coefficients.

Assuming that at the boundaries of the two media, nanoparticle and host, the tangential part of the electric and magnetic field is continuous we can solve the boundary problem. Finally we derive such equations for the Mie coefficients [35]:

$$a_n = \frac{\psi_l(x)\psi_l'(mx) - m\psi_l(mx)\psi_l'(x)}{\xi_l(x)\psi_l'(mx) - m\psi_l(mx)\xi_l'(x)}, \tag{42}$$

$$b_n = \frac{m\psi_l(x)\psi_l'(mx) - \psi_l(mx)\psi_l'(x)}{m\xi_l(x)\psi_l'(mx) - \psi_l(mx)\xi_l'(x)}, \tag{43}$$

where $m = m_{real} + im_{im}$ is the complex refractive index of nanoparticle and m_{im} is imaginary part of refractive index, $\psi_l(x)$ spherical Bessel function of the first kind and $\xi_l(x)$ Ricatti-Bessel functions. $\psi_l'(x)\,\&\,\xi_l'(x)$ are their derivatives with respect to x. Equations for Bessel functions are such:

$$\psi_l(x) = \sqrt{\frac{\pi x}{2}}J_{l+0.5}, \tag{44}$$

$$\xi_l(x) = \psi_l(x) + \chi_l(x) = \sqrt{\frac{\pi x}{2}}\left(J_{l+0.5}(x) + iY_{l+0.5}(x)\right). \tag{45}$$

Here $J_l(x)$ represents a Bessel function of the first kind, $Y_l(x)$ a Bessel function of the second kind and $\chi_l(x)$ a spherical Bessel function of the second kind. In our approach Bessel function of second kind were calculated from the Bessel function of first kind [Appendix 1.1] and we did not use recursive approach. Deviation of our result from the result of the recursive approach, where the Bessel function of higher order is calculated on the basis of Bessel function of lower order [23], is not essential.

4. Short overview of metal nanoparticle-fluorophore interaction

4.1. Features of metal nanoparticle-fluorophore interaction

Fluorescence is an emission of light by an excited material having absorbed light or any other form of radiant energy. Usually the emitted light has longer wavelengths than the absorbed light, thus it is characterized by lower energies compared to the absorbed light. In rarer cases the emission can also be at the same wavelength as the absorbed light. This case is related to the resonance fluorescence [36].

In our experiments we used rare earth fluorescent ions, because they are characterized by high photostability. The efficiency of fluorescent materials can be understood as a part of the energy that's emitted in comparison with the absorbed one. The efficiency of fluorescent centre is dependent on several parameters. Let's consider them sequentially starting from the absorption cross section σ_{abs}.

As the molecule absorbs energy it enters to an excited state. Due to the principle of minimum energy, the system tends to have the lowest possible energy. So it goes down to its ground state by two channels. The first one is radiative Γ_{rad}, which results in fluorescent light. The second channel is nonradiative Γ_{nonrad} (Fig. 10). From this process we could calculate the quantum yield η [37] in form of:

$$\eta = \frac{\Gamma_{rad}}{\Gamma_{rad} + \Gamma_{nonrad}}, \tag{46}$$

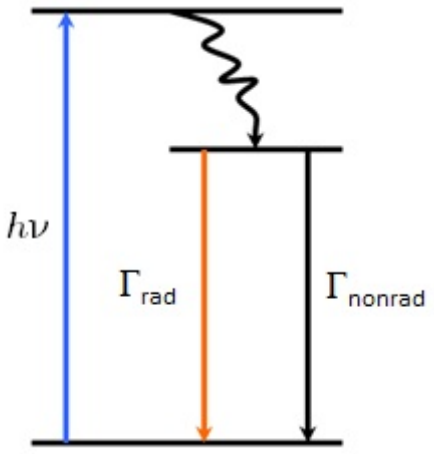

Fig. 10. Schematic representation of the excitation and decay processes visualised with a simplified Jablonski diagram.

However, in our experiments we tried to place noble metal nanoparticles close to the fluorophore molecules to improve the quantum yield of fluorescence. It is possible if the metal will provide more dominance of the radiative processes over the nonradiative. If the metal nanoparticle is placed close to the fluorescent molecule then we will typically have three main interactions [38]. These are: the changes of radiative rates which would increase or decrease the lifetime of fluorescence emission $\tau = 1/(\Gamma_{rad} + \Gamma_{nonrad})$; resonant energy transfer from fluorophore to metal nanoparticle and lastly, the change of effective excitation cross-section of the fluorescent molecule σ_{abs}^{eff}.

Let's consider what happens with quantum yield when a small metal nanoparticle brought relatively close to a fluorescent molecule (Fig. 11) [39]. We can approximate situation by dipole-dipole interaction of fluorophore molecule and metal nanoparticle. Depending on the orientation of the dipoles and distances between them, their oscillations could be out-of-phase or in-phase. Out-of-phase situation results in decrease of total radiative rate. In-phase case could increase the radiative rate. In phase case constitutes to a situation where the fluorophore dipole moment is brought radially to the dipole moment of metal nanoparticle. But out-of-phase constitutes where it is brought tangentially close to the fluorophore.

Yet the nonradiative rate in this situation would increase in any case due to the fact that we will have to include energy transfer component Γ_{ET} in the nonradiative rate. Furthermore, energy transfer increases by decreasing distance. And even in the case of an 'in phase' situation, if the energy transfer is dominant then quantum efficiency still decreases. The nonradiative rate is then:

$$\Gamma_{nonrad} = \Gamma_{nonrad}^{o} + \Gamma_{ET} \,. \tag{47}$$

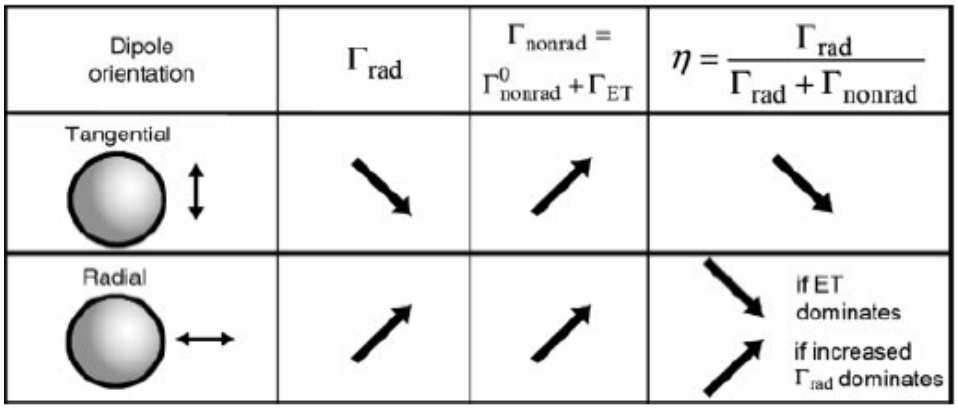

Fig. 11. Scheme of changes in the radiative, nonradiative rates and quantum yield for the fluorophore (double arrow) situating near the metal nano-particle [39].

Control of fluorophore radiative rate by placing it near the noble metal nanoparticle is a non-trivial theoretical and experimental task which is not solved in general form at present time. Theoretically,

it can lead to the uncovering of novel effects of fluorescent light coupling with matter oscillations that could provide new options for the creation of nanooptical elements such as nanolasers [40]. Experimentally, metal enhanced fluorescence is becoming a basis for the fluorescent sensing and lighting materials with improved efficiency. The next paragraph describes briefly a state of the art and current problems in the field of fluorescence controlled by metal nanoparticles.

4.2. Review of current problems of plasmon coupled fluorescence

While in the previous chapter we considered what happens with the radiative rates and quantum yield, which determine the efficiency of fluorescent materials, if the metal nanoparticle was brought not very close to the fluorophore. Then the effects were quite easily understandable.

Fluorophore taken as emitting dipole induces charges in the metal in a mirror-like manner. Mentioned in paragraph 4.1 Sommerfeld's approach [39] together with consideration of ohmic losses in the metal [41] allow realistically predict the radiative and non-radiative rates of the fluorophore situating at the distances 10-150 nm from the metal. But at smaller distances we meet an additional complications in calculations connected with insufficient definition of macro parameters such as permittivity for the nanoscale objects.

Local electrodynamical theory becomes inapplicable at the nanoscale due to the fact that the dielectric permittivity varies at the surface roughnesses [42]. The randomness of metal roughness complicates calculation of related fluctuations of the metal permittivity at the nanoscale. Solution of the problem could be started from experimental investigations and related calculations for the single spherical metal nanoparticles with further generalization on the cases of complex shapes such as rods, pairs of nanoparticles and finally on the case of rough surface.

In general, electron density inside the polyatomic molecules of fluorophores is distributed asymmetrically. It is possible to approximate it by a system of several multipoles. In first approximation fluorophore can be considered as a dipole having two levels of energy. In this case the light induced mirror-like dipole in the nearby metal accepts energy from the fluorophore non-radiatively by Förster mechanism [43]. The Föster-type interplay itself considers that energy transfer is proportional to the inverse sixth power of the distance between the dipoles. It supposes that light absorption spectrum for metal nanoparticle and emission spectrum of the fluorescent molecule are partially overlapped. When decrease in distance between the fluorophore and metal becomes comparable with the size of molecule, contribution not only from dipole, but also from higher order multipoles inside fluorophore molecule should be taken into account. If distances become so small (<1nm) that different atoms can share certain excited electrons, exchange by

excited electron between the fluorophore and metal becomes possible. This interaction can be seen as Dexter-type energy transfer [44].

In many practical situations it is enough to consider numerical solutions of Maxwell equations [45] in static approximation, when dipole moment in the metal is induced by the excited fluorophore. This dipole moment affects radiative rate of the fluorophore. So consideration of total dipole moment for the fluorophore-nanoparticle composite can give an answer about increased or quenched fluorescence [45]. All in all this approach is similar to the theory of Rayleigh. It can be done for any complex shape of metal nanoparticles as long as the depolarisation coefficient is known [47]. But the most useful way to overcome the previous problem is to use a fully electrodynamic theory [46]. With what we can view components of quantum yield like a linear decomposition of electromagnetic field into spherical wave components. This approach is similar to the theory of Mie. But if we compare last two approaches with the experiments then they would work quite well on the scales for nanoparticle sizes and distances down to tens of nanometres. Since at distances less than 1 nm local theory becomes questionable [48].

A nice summary of fluorophore-metal interactions depending on the distances between them was done by Lackowicz [49] (Fig. 12). At first range of distances (≤ 50 Å) there is a quenching of fluorescence, which is caused mainly by Föster energy transfer from the fluorophore to metal and ohmic losses in the metal (Fig. 12, marked by k_m). At distances 50-150 Å the local electric field of metal nanoparticle increases and this causes an increase in absorption cross section and as consequence in fluorescent emission of fluorophore (Fig. 12, marked by E_m). For the last range of distances 150-250 Å plasmonically enhanced radiative rate for fluorophore can be obtained (Fig. 12, marked by Γ_m). In this case the effect of increase or decrease in fluorescence yield can be obtained depending on the predominance of radiative or nonradiative rates described in equations (46) and (47).

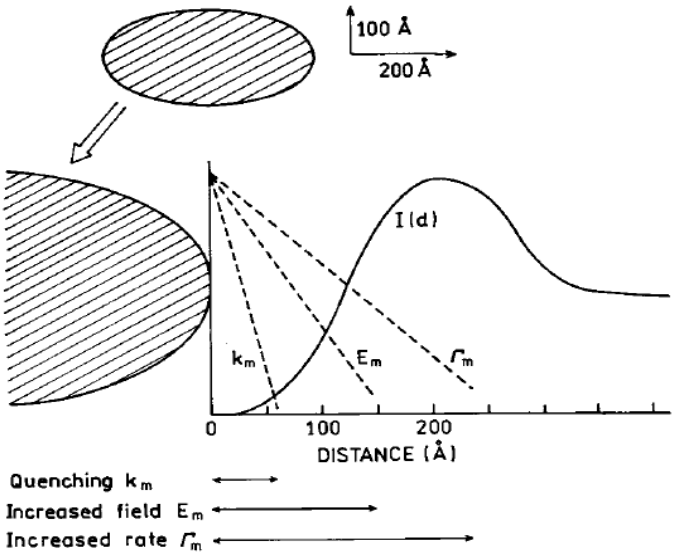

Fig. 12. Dependence of interaction influences on fluorescence by decreasing the distance between the fluorescent centre and the metal nanoparticle [49].

Quantitatively the contribution of different mechanisms to the total fluorescence yield can be represented by the equation [38]:

$$F(\lambda_{ex},\lambda_{em}) = \frac{\lambda_{ex} I(\lambda_{ex})}{hc} \sigma_{abs}^{eff}(\lambda_{ex}) \eta(\lambda_{em}), \tag{48}$$

where λ_{ex} & λ_{em} are the excitation and emission wavelengths, $I(\lambda_{ex})$ is the intensity of exciting light, $\eta(\lambda_{em})$ the quantum efficiency and $\sigma_{abs}^{eff}(\lambda_{ex})$ the effective absorption cross section. The latter value is different from the cross section of an undisturbed fluorescent centre, since placing a metal nanoparticle close to fluorescent centre changes the initial cross section. Connection between the plasmonically modified absorption cross section of fluorophore, its initial cross section and quantum yield can be represented by such a way [38]:

$$\sigma_{abs}^{eff}(\lambda_{ex}) = \frac{\left|\vec{p} \circ \vec{E}(\lambda_{ex})\right|^2}{\left|\vec{p} \circ \vec{E}^0(\lambda_{ex})\right|^2} \sigma_{abs}^{eff}(\lambda_{ex}), \tag{49}$$

where $\vec{p}$ is the molecular dipole moment, $\vec{E}$ and $\vec{E}^0$ are local fields with and without metal correspondingly. As in case of the emission rate, absorption cross section also depends on the light polarization, its wavelength and distance from the metal.

Dependence of fluorescence intensity on its wavelength can illustrate enhancement or quenching of light emission, but cannot give comprehensive information about the reasons for it. While time resolved fluorescence can provide the data about changes in the absorption cross section or radiative rate of fluorophore (Fig. 13) [38, 50-52]. Such measurement is conducted at certain fixed wavelength selected from the fluorescent spectrum.

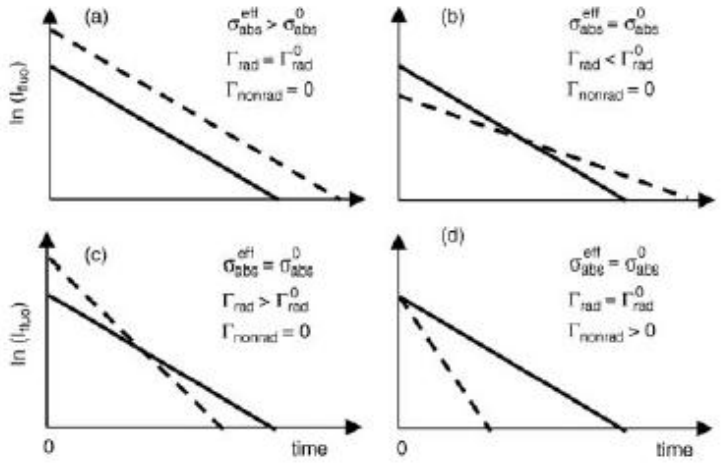

Fig. 13. Schemes of time kinetics for distinguishing changes in absorption cross section and radiative rate of fluorophore: (a) increase of absorption cross section; (b) decrease in radiative rate; (c) increase in radiative rate; (d) increase in non-radiative rate. Solid line (——) corresponds to the behavior of unperturbed fluorophore; dashed line (-------) is related to fluorophore near metal surface [38].

Let's comment sequentially each part in the Fig. 13. Intensity of light emitted at certain wavelength is proportional to the area of triangle restricted by coordinate axes and solid or dashed lines. For simplicity the non-radiative rate in Fig. 13, a-c is neglected, the equality or inequality of absorption cross sections and radiative rates are marked the Fig. 13 also.

A. The area under the dashed line is higher then under the solid line. It means that in the vicinity of the metal emitted energy is higher. Since the solid and dashed lines are parallel the emission life time is not changed and increase of fluorescence is caused only by the increase in absorption cross section.

B. A situation where by placing metal nanoparticles close to the fluorescence molecules we have decrease of radiative rate. Since even here nonradiative rates weren't considered there is no nonradiative energy transfer. If then radiative rate was decreased for the composite system by the plasmonic effects then the fluorescence decay time becomes longer, but the amount of energy, which it emits, stays the same as for the pure sample. This happens only if the intensity for the composite system in the beginning is smaller.

C. The opposite situation of the pervious one. Here we have increase of radiative rate by placing metal nanoparticles close to the fluorescent molecules. Like here without any nonradiative rate there is no nonradiative energy transfer. But the difference is that by increasing the fluorescence radiative rate by plasmonic effects the fluorescence has to decay faster. This happens only if the intensity in the beginning for the fluorescence is bigger for the composite system.

D. Amount of emitted energy and corresponding area under the dashed line become less, because energy from the fluorophore is non-radiatively transferred to the metal. Fluorescent lifetime decreases in this case.

So far the approximations were done for a weak regime, but for smaller distances, which are close to few nanometres we should also consider the changes in the emission and absorption spectrums.

The first problem lies with the consideration of absorption and emission spectra of the fluorophore as sharp lines compared to plasmonic resonance peaks. This is not true since they are also quite broad and affect each other. So it wouldn't be correct to calculate fluorescence yield wavelength by wavelength. The problem is similar to the Purcell effect. This is an effect that can be visualized by two mirrors and standing waves between them. If the integer amount of half wavelengths fits between the mirrors then there is an increase of emission rate. Thus each radiative decay channel is dependent on its surrounding channels. Since this effect changes radiative rates it also changes quantum efficiency to the form:

$$\eta(\lambda) = \frac{\Gamma_{rad}(\lambda)}{\int_o^\infty f(\lambda')\Gamma_{rad}(\lambda')d\lambda + \int_o^\infty f(\lambda')\Gamma_{ET}(\lambda')d\lambda' + \Gamma^o_{nonrad}}. \qquad (50)$$

Where $f(\lambda')$ is the integral of the normalized fluorescence spectrum of the isolated fluorescence.

As for the absorption spectrum the change occurs if the absorption spectrum of fluorophore overlaps with plasmon resonance. So well, that the eigenfrequencies in the system would start to shift. This effect is called anticrossing and it's similar to the Fano effect [53]. In the absorption spectrum it is seen as a red and blue shift depending on whether the coupling wavelength was to the left or right. The Fano effect can be shown in the following energy level scheme:

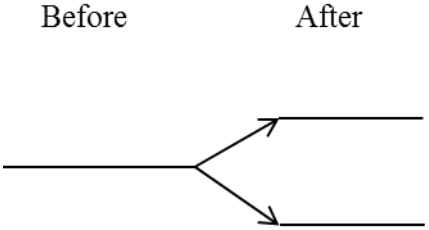

Fig. 14. Fano effect for absorption peaks being shifted away.

Further the original results connected with the experimental local enhancement of the Sm^{3+} rare earth fluorescence are reported.

5. Our original results and discussion

5.1. Size and concentration of metal nanoparticles by means of Mie theory

Spectral data about the light extinction in dispersions of metal nanoparticles is useful for the determination of the size of particles and their concentration in dispersion. The extinction of the light beam passing through the layer of dispersion can be illustrated in terms of the electric strength of incident wave [54]:

$$E(z,t) = \mathrm{Re}\left(E_0 e^{i(kz-wt)}\right) = e^{-\frac{2\pi m_{im}}{\lambda_0} z}\,\mathrm{Re}\left(E_0 e^{i(\frac{2\pi m_{real}}{\lambda_0} z - wt)}\right), \tag{51}$$

Thus the light intensity as a value proportional to the square of the electric strength can be represented in form of the Lambert-Beer law:

$$I = I_0 e^{-\alpha_{abs} z}, \tag{52}$$

where $\alpha_{abs} = \frac{4\pi m_{im}}{\lambda_0}$ is a coefficient related to the light absorption or in more general case to the light extinction. Light extinction consists of the sum of light scattering and light absorption. The Lambert-Beer law is more frequently applicable for the absorbing media. While in the Ref [7] it is shown that the Lambert-Beer equation can be used also in cases of light absorbing media with small light scattering. In this case the extinction coefficient is used instead of the absorption coefficient.
So the Lambert-Beer law can be represented as follows:

$$I = I_0 e^{-\rho C_{ext} L}, \tag{53}$$

where ρ is the concentration of absorbing particles, C_{ext} the extinction cross-section of one particle and $z = L$ is the optical path length.

Let's take into account that optical absorption *A* can be represented as:

$$A = -\log_{10}(\frac{I}{I_0}). \tag{54}$$

It is possible to derive concentration of the absorbing particles in the solution from (53) and (54) in form of:

$$\rho = \frac{2.303A}{C_{ext} L}. \tag{55}$$

Where L is the optical path length in cm.

In our case light absorption A(λ) spectrum measured for the water dispersion (n_{med} = 1.333) of gilded nanoparticles consists of a dipole at 680 nm and a quadrupole at 540 nm plasmonic resonant bands (Fig. 15). Taking the size of gold nanoparticles as 170 nm from the data of the scanning electron microscopy (Fig. 5) and the thickness of the sample equal to 1 cm, we can calculate using the Mie approach described in paragraph 3.3 the theoretical light extinction cross section C_{ext}. The theoretical line was multiplied by $(\times 10^{-14} - 0.32)$ to compare with the experimental result. As control points we can take the values of absorption coefficients *A*(680)=0.72 at the maximum point of the dipole band and *A*(540)=0.69 at the maximum point of the quadrupole band (Fig. 15). Then by substituting the theoretical cross sections σ_{ext} (680) and σ_{ext} (540) together with experimental absorption coefficients *A*(680) and *A*(540) to the equation (55) it is possible to calculate and compare the concentrations of particles ρ(680) and ρ(540). Indeed, calculations according to the (55) give us: $\rho(680)=1.483\times10^{9}\ \frac{particles}{cm^3}$ and $\rho(540)=1.565\times10^{9}\ \frac{particles}{cm^3}$. Comparison of our result with literary data [55] proves the reasonableness of our estimations.

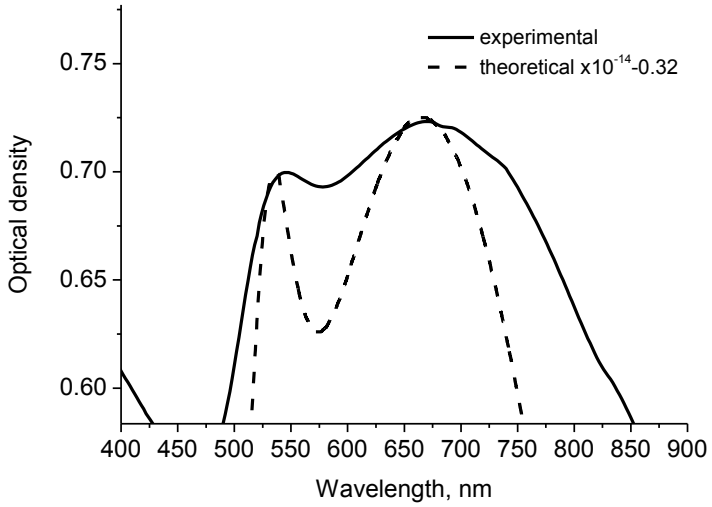

Fig. 15. Experimental (solid line) and theoretical (dashed line) absorption spectra (Mie Model) for the water dispersion of gilded nanoparticles. The radius of nanoparticle taken for the theoretical calculation is 85 nm.

5.2. Coloration of metal colloids. Dark field microscopy of nanoparticles

Dispersions of noble metal nanoparticles have colours in transmitted light, which are spectrally additional to the colours absorbed due to the plasmonic resonance. The colour of solids and liquids stained by noble metal nanoparticles is dependent on their shape and size. The light absorption by spherical gilded nanoparticles changes with their size. Plasmon resonance light absorption by

nanoparticles with sizes below 100 nm dispersed in water is situated near 520-540 nm, which corresponds to the absorption of greenish light. Together with the interband light absorption in the bluish range it results in the appearance of residual reddish colours typical for dispersions of small gold nanoparticles in transmitted light (Fig. 16, a). However light absorption by bigger gold nanoparticles is characterized by two peaks, quadrupole at 540 nm and a broader dipole peak at 650-750 nm that leaves mostly a dark blue colour in the spectrum of transmitted light (Fig. 16, b).

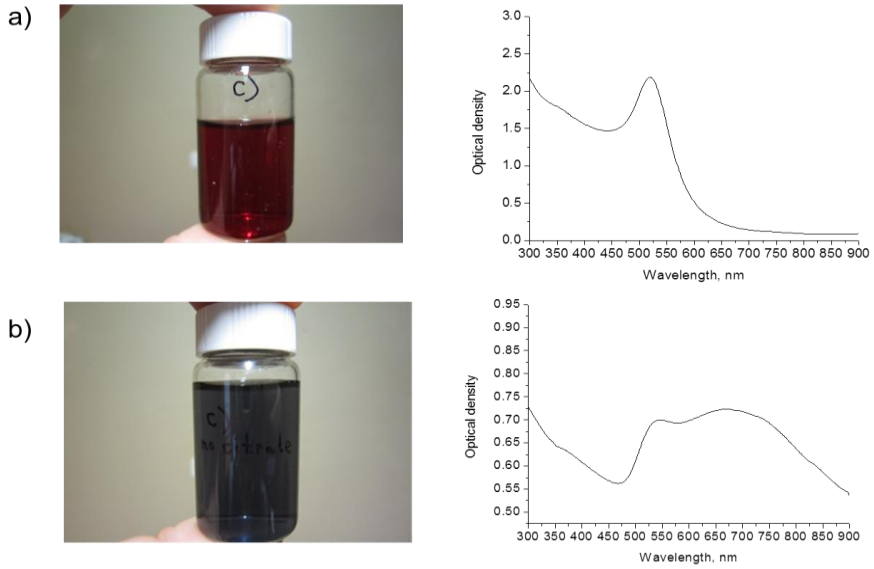

Fig. 16. Appearance and light absorption spectra of gold colloids in water for smaller (a) and bigger (b) nanoparticles.

There are several possible microscopic methods which can help us visualize the small nanoparticles which we have prepared. Here we used bright field and dark field microscopies. In principle these are low cost microscopy methods based on the use of visible light.

The working principle is following:

I. For a bright field.

a) Light source emits light to the condenser lens.

b) The light is focused on the sample and passed to the objective of the microscope where we see the image of our sample.

II. For a dark field.

a) Light source emits light to the condenser lens, but on the optical axis before the condenser there is a shutter that blocks the axial light beams.

b) The remaining non-blocked side beams of the light are focused and passed through the sample but misses the

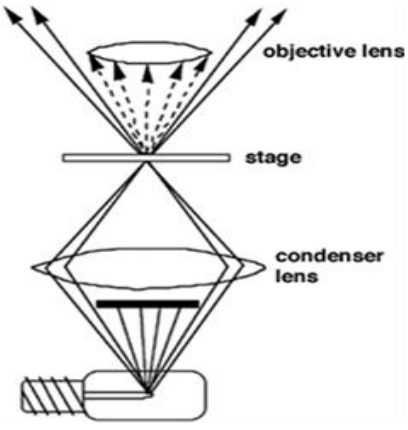

Fig.17. Scheme of Dark field microscopy setup.

objective. Therefore, the field of view is dark.

c) The bright spot on the dark field background appears only as a result of light scattering by a nanoparticle or an optical heterogeneity in the sample [56].

This microscopy technique itself is mainly used to enhance the contrast of the image, but the drawback is that the sample can be damaged by the quite strong illumination usually used.

If we compare the resulting dark field and bright field images one would appear just negative and the other one bright. However, there are also different effects detectable in both of them. For an example, the metal nanoparticles with sizes 50-100 nm are not visible with bright field microscopy due to the diffraction limit. This means that if the nanoparticle would be smaller than half of the visible light wavelength then it is not noticeable or it becomes fuzzy and is surrounded by diffraction rings called ‘Airy rings’. While in dark field our nanoparticles become visible because of two reasons: firstly, the method itself increased the resolution; secondly visualization is possible due to the light scattered by metal nanoparticle, which becomes visible on the dark background.

The small separated gold nanoparticles dispersed in the TiO_2 film give greenish-yellowish light scattering (Fig. 18, a), because the plasmon resonance scattering for them is situated at the greenish-yellowish spectral range 580-600 nm. It is easy to see knowing ε as refractive index squared for the TiO_2 and for the gold and using the equation (21). Presence of bigger aggregates of gilded nanoparticles results in the appearance of other colours of scattered light depicting a more complicated case of light scattering influenced by plasmonic multipoles induced in the bigger nanoparticles and their aggregates (Fig. 18, b).

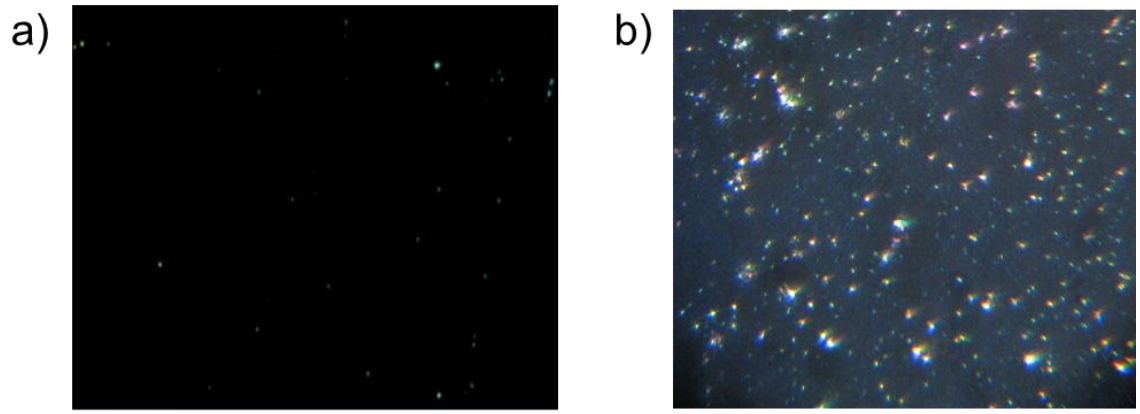

Fig. 18. Dark field microscopy for TiO_2 films doped with a) monodispersed and b) polydispersed gold nanoparticles.

5.3. Local enhancement of TiO_2:Sm^{3+} fluorescence in the vicinity of gilded nanoparticles

Planned experiment was aimed on analysis of rare earth fluorescence in the vicinity of gilded nanoparticles visualized by dark field light scattering. Single gilded nanoparticles look like colour spots on the dark background because of plasmonic light scattering in the dark field optical images (inset of Fig. 19, a). The corresponding fluorescence image under UV excitation shows bright red spots due to the fluorescent Sm^{3+} ions on the uniform fluorescent background. Generally, an excellent correspondence was revealed between the spots detected in dark-field scattering (Figure 19, a) and those observed in fluorescence (Figure 19, b). In contrast, in the samples without gold co-doping that were prepared in a similar way, no bright spots were observed in fluorescence. This is strong evidence about the plasmonic enhancement of Sm^{3+} fluorescence near the gilded nanoparticles.

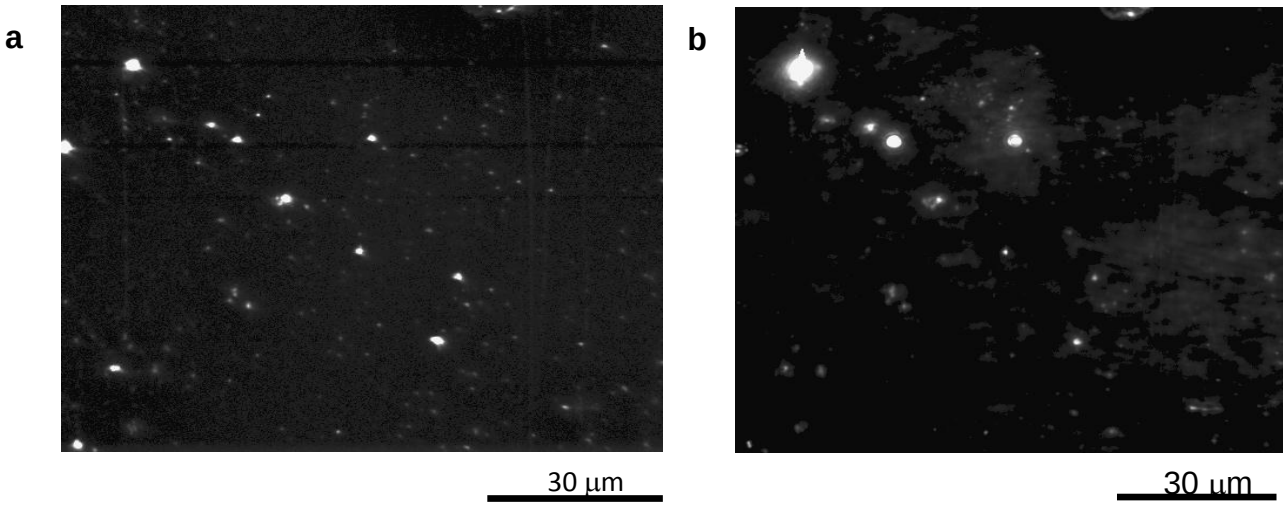

Fig. 19. Grayscale images of dark field light scattering (a) and fluorescence (b) from the TiO2:Sm3+-Au film (λ_{exc} = 355 nm).

The fluorescence spectrum under ultraviolet 355 nm excitation is typical for Sm^{3+} ions in crystalline anatase-type TiO_2 surrounding as evidenced by the crystal-field splitting of the four spectral bands due to the transitions $^4G_{5/2} \rightarrow {}^6H_{5/2}$, $^4G_{5/2} \rightarrow {}^6H_{7/2}$, $^4G_{5/2} \rightarrow {}^6H_{9/2}$, $^4G_{5/2} \rightarrow {}^6H_{11/2}$ of f electrons in Sm^{3+} ions. The intensity of the fluorescence at the bright spots near gilded nanoparticles is approximately 10 times higher than the background fluorescence of Sm^{3+} ions distant from metal inclusions (Fig. 20).

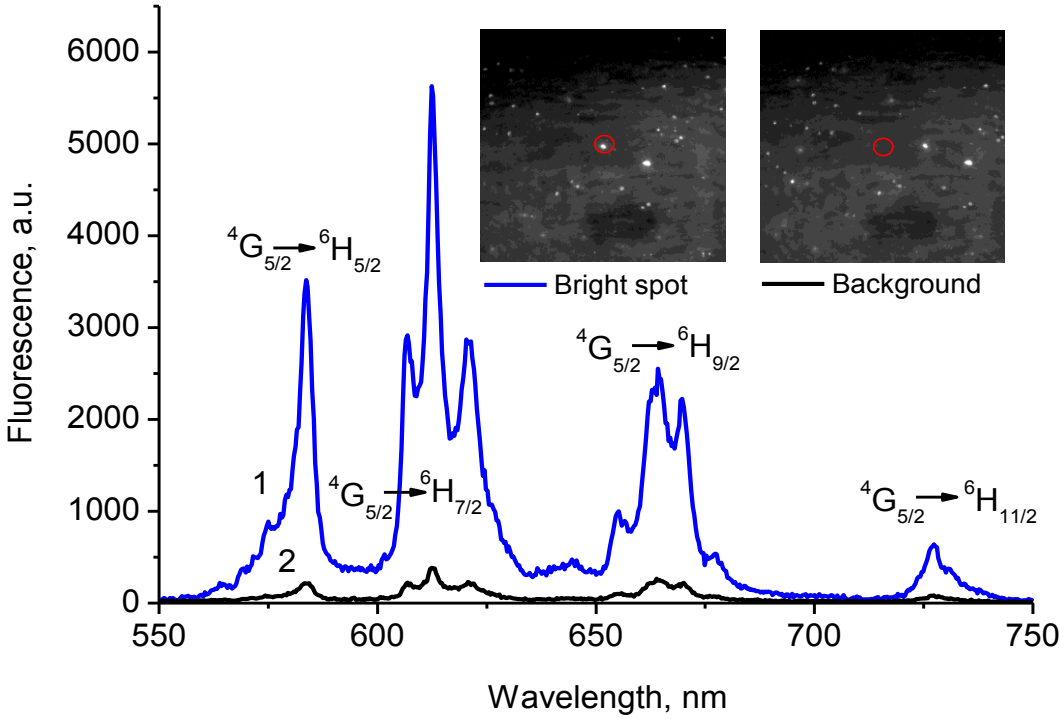

Fig. 20. Micro-luminescence spectra of TiO_2:Sm^{3+} films doped with gilded nanoparticles: (1) of bright spot, (2) background (λ_{exc} = 355 nm).

Plasmonic enhancement of fluorescence is usually explained either by an enhancement of light absorption or an enhancement of the radiative decay rate [37]. In the case of TiO_2, at least two different excitation mechanisms for rare earth ions must be distinguished (Fig. 21).

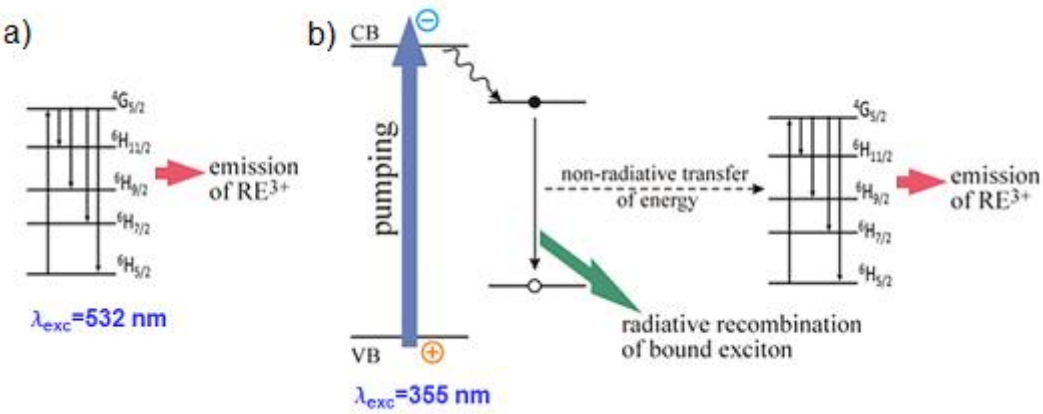

Fig. 21.a) direct and b) indirect ways for optical excitation of Sm^{3+} in TiO_2 host.

The first mechanism is realized when the absorption of ultraviolet light λ_{exc}=355 nm causes intrinsic excitations in TiO_2 host (the left part of the Fig. 21), such as the self-trapped or impurity-trapped excitons. These excitons can non-radiatively transfer energy to the fluorescent impurity. The effective cross section of such indirect Sm^{3+} excitation is several orders of magnitude higher than the direct absorption cross section 10^{-20}-10^{-21} cm^2 of Sm^{3+} ions for the visible light [57]. But

ultraviolet light cannot efficiently excite plasmon in the gilded nanoparticles due to the lack of resonance. So, the reasons for the enhancement of Sm^{3+} fluorescence are either a plasmonic enhancement of radiative decay rate or a plasmonically assisted energy transfer from the excitons to the Sm^{3+} ions. The fluorescent decay rate is inversely proportional to the fluorescent lifetime. To check the plasmonic influence on the decay rate, we measured the fluorescent kinetics for the bright spots and for the background rare earth fluorescence at the ultraviolet excitation λ_{exc} = 355 nm .(Fig. 22).

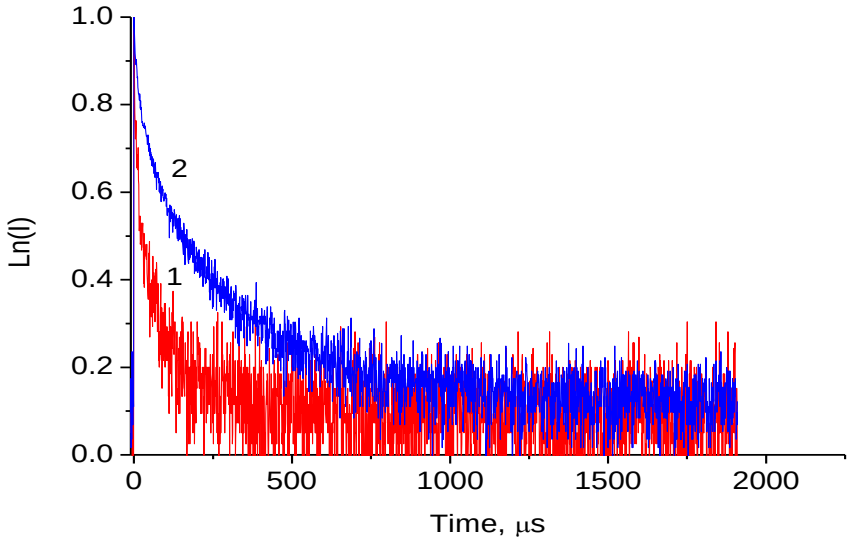

Fig. 22. Normalized experimental fluorescence decay kinetics: detected from background (1), from bright spot (2) of TiO_2:Sm^{3+} -Au films.

It was necessary to use up to three exponential decay components to satisfactorily model the kinetics:

$$I(t) = A_1 e^{\left(-\frac{t}{\tau_1}\right)} + A_2 e^{\left(-\frac{t}{\tau_2}\right)} + A_3 e^{\left(-\frac{t}{\tau_3}\right)}, \qquad (56)$$

where A_1, A_2 and A_3 are the coefficients of light intensity and τ_1, τ_2 and τ_3 are the lifetimes of fluorescence. In such a situation, the overall rate of decay is frequently characterized by the average lifetime defined as:

$$\langle \tau \rangle = \frac{\int_0^\infty tI(t)dt}{\int_0^\infty I(t)dt} = \frac{\sum_i A_i \tau_i^2}{\sum_i A_i \tau_i}. \qquad (57)$$

The obtained lifetimes of fluorescence are in the range of tens and hundreds of microseconds (Table 1). Fluorescence lifetimes of the order of hundreds of microseconds are typical for the rare earth ions situated in a good crystalline TiO_2 anatase host [57]. Lifetimes in the range of tens of

microseconds can be caused by Sm^{3+} fluorescent centres situated in the areas of TiO_2 host that have locally different crystallinity or local lattice defects. Corresponding lifetime components for the bright spots and for the background Sm^{3+} fluorescence are not very different. Based on this we can suppose that the radiative rate of rare earth fluorophore is not very strongly influenced by localized plasmons. Detected approximately 10 times enhancement in the intensity of Sm^{3+} fluorescence at the ultraviolet excitation could be caused by plasmonic support of energy transfer from excitons to rare earth ions. Possibility of non-radiative plasmonic support for the excitons was recently demonstrated in the case of plasmonically improved photocatalysis [58]. Plasmonic support of Förster resonance energy transfer for quantum dot's fluorescence was described in [59].

Place on the sample	τ_1, μs	τ_2, μs	τ_3, μs	τ, μs
Bright spot 1	2.4	25	156	103
Bright spot 2	6.5	48	299	147
Bright spot 3	10.5	78	294	202
Spot 1 on the background	4.1	35.3	225	138
Spot 2 on the background	7.4	50	220	137

Table 1**.** Lifetimes of fluorescence for the TiO_2:Sm^{3+} film doped with gilded nanoparticles, λ_{exc}= 355 nm.

Excitation by green light, λ_{exc} = 532 nm (right side of the Fig. 21), results in direct excitation of Sm^{3+} and also yields a fluorescence spectrum consisting of the four bands. But in this case, the bands are broader and almost featureless (Fig. 23).

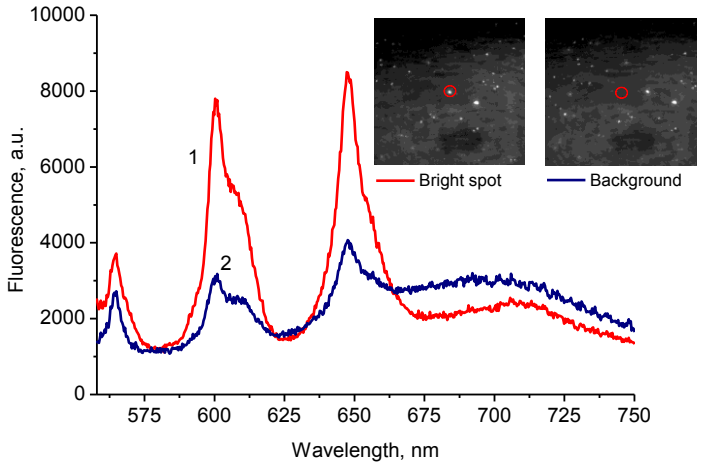

Fig. 23. Micro-luminescence spectra of TiO_2:Sm^{3+} films doped with gilded nanoparticles: (1) bright spot, (2) background (λ_{exc} = 532 nm).

It means that a different ensemble of Sm^{3+} ions is excited in this case. The absence of spectral features suggests that those Sm^{3+} ions are situated in less ordered TiO_2 environment [60]. In spite of the exclusion of excitonic influence at such excitation, we still detected a 2.5 times enhancement of fluorescence in the vicinity of gilded nanoparticles (Fig. 23). Under a 532 nm excitation the Stokes shift of the fluorescence emission is very small [61]. So, both excitation and emission can be influenced by plasmons. Fluorescence lifetimes at 532 nm excitation were measured in the spectral range of 580 to 660 nm. The obtained fluorescence decay is also multiexponential because different Sm^{3+} centres situate in TiO_2 environment with different local surroundings. Numerical values of the lifetimes are similar to those presented in Table 1. Because of the insignificant changes in the lifetimes of Sm^{3+} fluorescence, we suppose that the 2.5 times enhancement detected in the intensity of fluorescence could be caused mainly by the plasmon-enhanced direct absorption of exciting light by Sm^{3+} ions near the gilded nanoparticles.

6. Summary

Plasmon-enhanced fluorescence in TiO2:Sm^{3+} films co-doped with gilded silica nanoparticles

In this thesis the possibilities to enhance the fluorescence of trivalent samarium ions with the help of plasmonic resonance of gilded core-shell silica nanoparticles were studied. The results of measurements and calculations are presented.
Comprehensive review about the plasmonic resonance in noble metals and its manifestations in the light scattering, absorption and extinction (incl. Rayleigh and Mie theories) as well as in fluorescence was compiled on the basis of the available literature.

The original results achieved in the work can be summarized as follows:

1. Sol-gel synthesis was successfully adjusted to incorporate silica-gold core-shell nanoparticles into TiO_2:Sm^{3+} films.
2. An algorithm for the calculations of light absorption, scattering and extinction cross sections for the metal nanoparticle was elaborated and realized in the form of a Mathcad worksheet. The algorithm is based on the Mie light scattering theory. Unlike the generally approach it does not use a routine recurrent approach to calculate the Bessel functions. The inaccuracy of the result is comparable to the one that can be obtained by the recurrent approach.
3. It is shown how to match Mie calculations with experimental data. That allows estimation of the size and concentration of noble metal nanoparticles in the liquid solution. Experimental skills to visualize metal nanoparticles by dark field microscopy method were obtained. Coloration of metal colloids was explained in view of the plasmonic resonance causing light extinction.
4. Prospective capabilities of these particles for the local plasmonic enhancement of rare earth fluorescence were demonstrated. We detected 10 times locally stronger Sm^{3+} fluorescence near the gilded nanoparticles under 355 nm excitation. However, fluorescent lifetimes were not changed significantly. It was concluded that phenomenon is more connected with plasmonic improvement of energy transfer from the excitons to the Sm^{3+} ions. Detected 2.5 times enhancement of Sm^{3+} fluorescence under 532 nm excitation can be caused by the plasmonic enhancement of direct light absorption by Sm^{3+} ions.

7. Kokkuvõte

Ülekullatud ränidioksiidi osakestega kaasdopeeritud TiO2:Sm^{3+} kilede plasmonvõimendatud fluorestsents

Siim Heinsalu

Käesolevas töös on uuritud Sm3+ ioonide fluorestsentsi võimendumist, mis on esile kutsutud ülekullatud räniosakeste pinnaplasmon resonantside poolt. Töö koosneb protsesside ülevaatest ja originaalsest eksperimentaalsest osast.

Töö algab pinnaplasmonite ja fluorestsentsinähtuste teoreetilisest käsitlusest. Kirjeldatakse füüsikalisi aluseid, kuidas metallosakesed interakteeruvad valgusega läbi plasmonneeldumise ja -hajumise. Nähtuste kirjeldamiseks tutvutakse Rayleigh'i ja Mie hajumisteooriatega. Seejärel antakse lühike ülevaade fluorestsentsist ja selle matemaatilisest kirjeldamisest.

Töö eksperimentaalses osas kirjeldatakse uuritud objektide valmistamist ning vajaminevate mõõtmiste metoodikaid. Mõõtmiste tulemusi analüüsitakse ning seletatakse eelnevalt kirjeldatud teooriatega.

Töö põhilised saavutused on:

1. Valmistati Mie hajumisteoorial põhinev Mathcad-i tööleht arvutamaks nanometallkuulide neeldumise, hajumise ja ekstinktsiooni ristlõikeid.

2. Mõõdetud läbilaskvusspektrite põhjal hinnati prekursorlahuses olevate nanometallkuulide kontsentratsiooni ja suuruste jaotust.

3. Saavutati oskuseid visualiseerida metallist nanoosakesi tumevälja mikroskoopia abil. Metallide värvust seletati plasmonresonantsi efektidega nanoosakestes.

4. Omandati praktilised oskused ülekullatud räni nanoosakeste valmistamiseks ja nendega TiO2:Sm3+ kilede kaasdopeerimiseks kasutades ja sool- geel meetodikat.

5. Demonstreeriti räni-kuld tuum-kest nanoosakeste sobivust haruldaste muldmetallide fluorestsentsi võimendamiseks. Eksperimentaalselt on näidatud Sm3+ ioonide emisiooni võimendamist kuni 10 korda ergastava lainepikkuse λ_{exc}=355 nm korral. Kuna kiirguse eluiga ei muutunud, siis järeldati, et efekti füüsikaline sisu on plasmonefektide poolt esilekutsutud ergastusenergia ülekande suurenemine TiO_2 keskkonnalt Sm^{3+} ioonidele. Ergastava lainepikkuse λ_{exc}=532 nm korral mõõdeti 2,5 kordne fluorestsentsi võimendus, mis on arvatavasti põhjustatud plasmonefektide poolt esilekutsutud valguse neeldumise suurenemisest.

8. Acknowledgments

The author would like to thank his colleagues Kathriin Utt, Valter Kiisk and Ardi Loot, from Laboratory of Laser Spectroscopy, Martin Timusk and Siim Pikker from Laboratory of Physics of Nano Structures for the help to make the samples and perform experiments. As well for the advices they have given.

Most especially his supervisors Leonid Dolgov and Ilmo Sildos, for the support and educational discussions throughout the preparation of the following thesis.

And finally his parents whose support made it possible to commit on the studies.

9. References

[1] I. Freestone, N. Meeks, M. Sax, C. Higgitt, "The Lycurgus Cup – A Roman Nanotechnology" // Gold Bulletin, Volume 40, Issue 4, p. 270-277, 2007. DOI: 10.1007/BF03215599

[2] M. Faraday, "The Bakerian lecture: experimental relations of gold (and other metals) to light" // Philosophical Transactions of the Royal Society of London, Vol. 147, p. 145-181, 1857. DOI: 10.1098/rstl.1857.0011

[3] R. W. Wood, "On a Remarkable Case of Uneven Distribution of Light in a Diffraction Grating Spectrum" // Proceedings of the Physical Society, vol. 18, p. 269-275, 1902. DOI:10.1088/1478-7814/18/1/325

[4] G. Mie, "Beiträge zur Optik trüber Medien speziell kolloidaler Goldlösungen" // Annalen der Physik, vol. 330, Issue 3, pp.377-445, 1908. DOI: 10.1002/andp.19083300302

[5] A. Polman, "Plasmonics Applied" // Science, Vol. 322, Issue 5903, p. 868-869, 2008. DOI: 10.1126/science.1163959

[6] W. Nomura, M. Ohtsu, T. Yatsui, "Nanodot coupler with a surface plasmon polariton condenser for optical far/near-field conversion" // Appl. Phys. Lett. Vol. 86, p. (181108-1)-(181108-3), 2005. DOI: 10.1063/1.1920419

[7] J. Yguerabide, E. Yguerabide, "Light-scattering submicroscopic particles as highly fluorescent analogs and their use as tracer labels in clinical and biological applications: II. Experimental Characterization"// Analytical Biochemistry, Vol. 262, Issue 2, p. 157-176, 1998. DOI: 10.1006/abio.1998.2760

[8] S. Kruszewski, T. Wybranowski, M. Cyrankiewicz, B. Ziomkowska, A. Pawlaczyk, "Enhancement of FITC Fluorescence by Silver Colloids and Silver Island Films" // Acta Physica Polonica A, vol. 113, Issue 6, p.1599-1608, 2008. BIO: 2008AcPPA.113.1599K

[9] H. Kozuka, "Metal nanoparticles in gel-derived oxide coating films: Control and Application of surface plasma resonance" // Proceedings of SPIE, vol. 3136, p. 304-314, 1997. DOI: 10.1117/12.279166

[10] A. C. Marques, R. M. Almeida, “Er photoluminescence enhancement in Ag-doped sol–gel planar waveguides” // Journal of Non-Crystalline Solids, vol. 353, Issue 27, p. 2613–2618, 2007. DOI:10.1016/j.jnoncrysol.2007.05.010

[11] S. Pikker, L. Dolgov, S. Heinsalu, S. Mamykin, V. Kiisk, S Kopanchuk, R. Lõhmus, I. Sildos, “Gilded nanoparticles for plasmonically enhanced fluorescence in TiO2:$Sm3^{+}$ sol-gel films” // Nanoscale Research Letters, vol. 9, Issue, p.143, 2014. DOI:10.1186/1556-276X-9-143

[12] www.bell-labs.com/org/physicalsciences/projects/solgel/solgel.html

[13] C. J. Brinker, G. W. Scherer, “Sol-Gel Science: The Physics and Chemistry of Sol-Gel Processing” – Academic press inc., 1990. ISBN-10: 0121349705

[14] A. Einstein, “Zur Theorie der Brownschen Bewegung” // Annalen der Physik, vol. 19, p. 371-381, 1906. DOI:10.1002/andp.19063240208

[15] W. Ströber, A. Fink, “Controlled Growth of Monodisperse Silica Spheres in the Micron Size Range” // Journal of Colloid and Interface Science, vol. 26, Issue 1, p. 62–69, 1968. DOI: 10.1016/0021-9797(68)90272-5

[16] T. Pham, J. B. Jackson, N Halas, T. R. Lee, “Preparation and characterization of gold nanoshells coated with self-assembled monolayers”// Langmuir, vol. 18, Issue 12, p. 4915-4920, 2002. DOI: 10.1021/la015561y

[17] S. J. Oldenburg, R. D. Averitt, S. L. Westcott, N. J. Halas, “Nanoengineering of optical resonances” // Chemical Physics Letters, vol. 288, Issue 2-4, p. 243-247, 1998. DOI: 10.1016/S0009-2614(98)00277-2

[18] P. C. Hieminz, R. Rajagopalan, “Principles of Colloid and Surface Chemistry” – Marcel Dekker Inc., 1986. ISBN-10: 0824793978

[19] M. Born, E. Wolf, “Principles of optics: Electromagnetic theory of propagation, interference and diffraction of light” – Cambridge University Press, 1999. ISBN-10: 9780521642224

[20] P. Drude, “Zur Elektronentheorie der Metalle“ // Annalen der Physik, vol. 306, Issue 3, p. 566–613, 1900. DOI: 10.1002/andp.19003060312

[21] U. Mizutani, “Introduction to the Electron Theory of Metals” – Cambridge University Press, 2001. ISBN-10: 0521587093

[22] W. Cai, V. Shalaev, “Optical Metamaterials Fundamentals and Applications” – Springer, 2010. ISBN-10: 1441911502

[23] C. F. Bohren, D. R. Huffman, “Absorption and Scattering of Light by Small Particles” – Wiley-VCH, 1983. ISBN-10: 0471293407

[24] W. J. Duffin, “Electricity and magnetism” – McGraw-Hill Publishing Co., 1980. ISBN-10: 007084111X

[25] irina.eas.gatech.edu/ATOC5235_2003/Lec9.pdf

[26] S. K. Friedlander, “Light scattering” in “Smoke, dust, and haze: fundamentals of aerosol dynamics” – Oxford University Press, 2000. ISBN-10: 0195129997

[27] S. Link, M. A. El-Sayed, “Size and Temperature Dependence of the Plasmon Absorption of Colloidal Gold Nanoparticles” // Journal of Physical Chemistry B, vol. 103, Issue 21, p. 4212-4217, 1999. DOI: 10.1021/jp984796o

[28] www.lightscattering.de/MieCalc/index.html

[29] www.philiplaven.com/mieplot.htm

[30] B. S. Luk’yanchuk, M. I. Tribel’skii, V. V. Ternovskii, “Light scattering at nanoparticles close to plasmon resonance frequencies” // Journal of Optical Technology, Vol. 73, Issue 6, p. 371-377, 2006. DOI:10.1364/JOT.73.000371

[31] P. W. Barber, S. C. Hill, “Light Scattering by Particles: Computational Methods” – World Scientific Publishing Co Inc., 1998. ISBN-10: 9971508133

[32] Z. Meng, P. Yang, G. W. Kattawar, L. Bi, K.N. Liou, I. Laszio, “Single-scattering properties of tri-axial ellipsoidal mineral dust aerosols: A database for application to radiative transfer calculations” // Journal of Aerosol Science, vol. 41, Issue 5, p. 501–512, 2010. DOI:10.1016/j.jaerosci.2010.02.008

[33] plaza.ufl.edu/dwhahn/Rayleigh%20and%20Mie%20Light%20Scattering.pdf

[34] J. Yguerabide, E. Yguerabide, "Light-scattering submicroscopic particles as highly fluorescent analogs and their use as tracer labels in clinical and biological applications: I. Theory" // Analytical Biochemistry, vol. 262, Issue 2, p. 137-156, 1998. DOI: 10.1006/abio.1998.2759

[35] L. N. Ng, "Manipulation of particles on optical waveguides" / Ph.D. *thesis*, University of Southampton, *2000. ePrint ID:15499*

[36] A. Douglas, F. Skoog, J. Holler, S. R. Crouch, "Principles of Instrumental Analysis" – Brooks Cole, 2006. ISBN-10: 0495012017

[37] T. K. Sau, A. L. Rogach, "Complex-shaped metal nanoparticles bottom-up syntheses and applications"– Wiley-VCH, 2012. ISBN-10: 3527330771

[38] T. A. Klar, J. Feldman, "Fluorophore–Metal Nanoparticle Interactions and Their Applications in Biosensing" in "Complex-Shaped Metal Nanoparticles: Bottom-Up Syntheses and Applications" – Wiley-VCH Verlag GmbH & Co. KGaA, 2012. DOI: 10.1002/9783527652570.ch12

[39] A. Sommerfeld, "Über die Ausbreitund der Wellen in der drahtlosen Telegraphie" // Annalen der Physik, vol. 333, Issue 4, p. 665–736, 1909. DOI: 10.1002/andp.19093330402

[40] M. I. Stockman, "Spasers explained" // Nature Photonics, vol 2, p. 327-329, 2008. DOI:10.1038/nphoton.2008.85

[41] R. R. Chance, A. Prock, R. Silbey, "Molecular Fluorescence and Energy Transfer Near Interfaces", in "Advances in Chemical Physics" – John Wiley & Sons, Inc., New York, p. 1–65, 1978. DOI: 10.1002/9780470142561.ch1

[42] J. Arias, P. K. Aravind, H. Metiu, "The fluorescence lifetime of a molecule emitting near a surface with small, random roughness" // Chemical Physics Letters., 85, 404–408, 1982. DOI: 10.1016/0009-2614(82)83481-7

[43] T. Förster, "Zwischenmolekulare Energiewanderung und Fluoreszenz" // Annalen der Physik, vol 2, Issue 5, p. 55–75, 1948. DOI:10.1002/andp.19484370105

[44] D.L. Dexter, “A theory of sensitized luminescence in solids” // The Journal of Chemical Physics, vol. 21, p. 836-850, 1953. DOI: 10.1063/1.1699044

[45] J. Gersten, A. Nitzan, “Spectroscopic properties of molecules interacting with small dielectric particles“ // The Journal of Chemical Physics, vol. 75, Issue 3, p. 1139–1152, 1981. DOI: 10.1063/1.442161

[46] R. Ruppin, “Decay of an excited molecule near a small metal sphere” // The Journal of Chemical Physics, vol. 76, Issue 4, p. 1681-1684, 1982. DOI: 10.1063/1.443196

[47] R. Gans, “Strahlungsdiagramme ultramikroskopisher Teilchen” // Annalen der Physik, vol. 381, Issue 1, 29–38, 1925. DOI: 10.1002/andp.19253810103

[48] H. Metiu, “Surface enhanced spectroscopy“ // Progress in Surface Science , vol 17, p. 153–320, 1984. DOI: 10.1016/0079-6816(84)90017-0

[49] J. R. Lakowicz, “Radiative Decay Engineering: Biophysical and Biomedical Applications” // Analytical Biochemistry, vol. 298, p. 1-24, 2001. DOI: 10.1006/abio.2001.5377

[50] V. Kiisk, M. Šavel, V. Reedo, A. Lukner, I. Sildos, “Anatase-to-rutile phase transition of samarium-doped TiO_2 powder detected via the luminescence of Sm^{3+}” // Physics Procedia, vol 2, Issue 2, p. 527-538, 2009. DOI:10.1016/j.phpro.2009.07.038

[51] E. Dulkeith, M. Ringler, T. A. Klar, J. Feldmann, A. Munoz Javier, W.J. Parak, “Gold Nanoparticles Quench Fluorescence by Phase Induced Radiative Rate Suppression” // Nano Letters, vol. 5, Issue 4, p. 585–589, 2005. DOI: 10.1021/nl0480969

[52] F.R. Aussenegg, A. Leitner, M.E. Lippitsch, H. Reinisch, M. Riegler, “Novel aspects of fluorescence lifetime for molecules positioned close to metal surfaces” // Surface Science, vol. 189-190, p. 935–945, 1987. DOI: 10.1016/S0039-6028(87)80531-9

[53] U. Fano, “Effects of Configuration Interaction on Intensities and Phase Shifts” // Phys. Rev., vol. 124, Issue 6, p. 1866-1878, 1961. DOI: 10.1103/PhysRev.124.1866

[54] I. Gerhardt, “Scattering & Absorption of Light by a Single Molecule under a subwavelength Aperture” / PhD thesis, University Berlin, 2006. DOI: 10.3929/ethz-a-005279519

[55] www.bbisolutions.com/support/technical-information/molar-concentration-of nanoparticles

[56] www.ruf.rice.edu/~bioslabs/methods/microscopy/dfield.html

[57] G. Liu, B. Jacquier, "Spectroscopic properties of rare earths in optical Materials" – Springer Series in Materials Science, 2005. ISBN-10: 3540238867

[58] E. Liu , L. Kang , F. Wu, T. Sun ,X. Hu ,Y. Yang, H. Liu , J. Fan, "Photocatalytic reduction of CO2 into methanol over Ag/TiO2 nanocomposites enhanced by surface plasmon resonance" // Plasmonics, vol. 9, Issue 1, p. 61–70, 2014. DOI: 10.1007/s11468-013-9598-7

[59] T. Ozel, P. Hernandez-Martinez, E. Mutlugun , O. Akin, S. Nizamoglu , I. Ozel, Q. Zhang, Q Xiong, H. Demir, "Observation of selective plasmon-exciton coupling in nonradiative energy transfer: donor-selective versus acceptor-selective plexcitons" // Nano Letters , vol. 13, Issue 7, p. 3065–3072, 2013. DOI: 10.1021/nl4009106

[60] M. Elisa, I. Vasiliu, C. Grigorescu, B. Grigoras, H. Niciu, D. Niciu, A. Meghea, N. Iftimie, M. Giurginca, H. Trodahl, M. Dalley, "Optical and structural investigation on rare-earth-doped aluminophosphate glasses" // Optical Materials, vol. 28, Issue 6–7, p. 621–625, 2006. DOI: 10.1016/j.optmat.2005.09.030

[61] B. Henderson, G. F. Imbush, "Optical Spectroscopy of Inorganic Solids" // Clarendon Press, 1989. ISBN-10: 0521804841

[62] Kreh M. "Bessel Functions" // Project for the Penn State - Göttingen Summer School on Number Theory, 2012.

10. Appendix 1 - Calculations for Mie theory

The following appendix was done in Mathcad version 15. As such the equations are in Mathcad format.

$Au =$

	0	1	2
0	476.87	1.242	1.796
1	494	1.087	1.797
2	495.94	0.916	1.84
3	506.06	0.755	1.956
4	516.6	0.608	…

In the upper table the rows have following meanings:

0) wavelength;

1) real part of the refractive index;

2) imaginary part of the refractive index.

Following table values are for gold. For another metal just change the values.

Number of rows in the table:

$$v = 0,1..457 .$$

Real part of refractive index:

$$U = Au^{\langle 1 \rangle} .$$

Imaginary part of refractive index:

$$B = Au^{\langle 2 \rangle} .$$

Wavelength is given in meters:

$$\lambda = Au^{\langle 0 \rangle} \cdot 10^{-9} .$$

Refractive index of particle with respect to medium:

$$n_v = \frac{U_v + iB_v}{n_m} .$$

Size parameter:

$$x_v = \frac{2\pi R n_{med}}{\lambda v} .$$

Changeable parameters:

Refractive index of medium:

$$n_{med} = 1.333.$$

Size of nanoparticle in dimensionless meter scale:

$$R = 100 \cdot 10^{-9}.$$

Approximation to l_{max} (maximum dipole order which is needed)

Approximation equation from [34]:

$$x_{ev} = \left[x_v + 4(x_v)^{\frac{1}{3}} + 2 \right].$$

Dependent on all values in s we need the maximum:

$$\begin{aligned} l_{\max}(nr, G) &= i \leftarrow 0 \\ &\quad a \leftarrow G_0 \\ &\quad \text{for } i \in G \\ &\quad a \leftarrow i \text{ if } |nr - a| < |nr - i| \\ &\quad \text{return } a \end{aligned} .$$

Rounding to the integer:

$$G_v = floor(x_{ev}).$$

For simplification we use also the wavenumber K:

$$K_v = \frac{2\pi m_m}{\lambda_v}.$$

Following Bessel equations were taken in form of ref [62].

Bessel Function of the first kind:

$$J(l, z) = \sum_{m=0}^{50} \left[\frac{(-1)^m}{m! \cdot \Gamma(m + 1 + l)} \left(\frac{z}{2} \right)^{2m+1} \right].$$

Number 50 was chosen as a value where one could calculate accurate enough results.

To prove this we have the following example. We find the maximum value of our parameters and see how well it corresponds to the built in Bessel equation.

$$F_v = x_v n_v \qquad \max(F) = 1.636 + 4.143i.$$

Supposing the maximum dipole order is up to 15:

$$l = 1..15.$$

Difference of the maximum values is:

$$D_l = J(l, \max(F)) - Jn(l, \max(F)) \qquad \max(D) = 2.665i \cdot 10^{-15}.$$

This shows us that the discrepancy is a really small value, thus the estimation is quite correct.

In Mie theory we use the Spherical Bessel functions so for the first kind of Spherical Bessel function we have:

$$\psi(l, z) = \sqrt{\frac{\pi z}{2}} J(l + 0.5, z).$$

First order derivative from it:

$$\Psi(l, z) = \frac{d}{dz} \psi(l, z).$$

Subsequently for the spherical Bessel function of the second kind we have:

$$\zeta(l, z) = \sqrt{\frac{\pi z}{2}} H(l + 0.5, z),$$

where $H(l, z) = J(l, z) + iY(l, z)$ is the Henekel-Bessel function. And $Y(l, z)$ is the Bessel function of the second kind. With the relations of the Bessel functions of the first and second kind we can the simplify Spherical Bessel function to the following:

$$\zeta(l, z) = \sqrt{\frac{\pi z}{2}} J(l + 0.5, z) + i\sqrt{\frac{\pi z}{2}} \begin{pmatrix} J(-l - 0.5, z) & \text{if} \quad \text{mod}(1,2) = 1 \\ -J(-l - 0.5, z) & \text{if} \quad \text{mod}(1,2) = 0 \end{pmatrix}.$$

First order derivative from it:

$$\xi(l, z) = \frac{d}{dz} \zeta(l, z).$$

To show how the previous equation was obtained we used two relations between the first and second kind of Bessel functions.

Firstly we have the relation:

$$Y(l, z) = \frac{J(l, z)\cos(l\pi) - J(-l, z)}{\sin(l\pi)},$$

where in the case of $l = 0.5$ we would have $Y(0.5, z) = J(-0.5, z)$.

And secondly:

$$-Y[(l + 0.5), z] = J[-(l + 0.5), z] \,\&\, Y[-(l + 0.5), z] = J[(l + 0.5), z].$$

Here we see that if the dipole order is even then we need to also add a minus sign. And by combining the two changes we can present the Spherical Bessel function of the second kind as:

$$\zeta(l, z) = \sqrt{\frac{\pi z}{2}} J(l + 0.5, z) + i\sqrt{\frac{\pi z}{2}} \begin{pmatrix} J(-l - 0.5, z) & \text{if} \quad \text{mod}(1,2) = 1 \\ -J(-l - 0.5, z) & \text{if} \quad \text{mod}(1,2) = 0 \end{pmatrix}.$$

The deducted function is also compared with the build Spherical Bessel function of the second kind.

The maximum parameter value:

$$F_v = x_v n_v \qquad \max(F) = 1.636 + 4.143i\,.$$

Supposing again that the maximum dipole order is up to 15:

$$w = 1..15\,.$$

The difference of the maximum values is:

$$O_w = Yn(w + 0.5, \max(F)) - \frac{Ys(w, \max(F))}{i\sqrt{\frac{\pi \max(F)}{2}}} \qquad \max(O) = 1.688 \cdot 10^{-9} + i2.9 \cdot 10^{-10}$$

As one can see, the discrepancy here is also a really small value.

Placing the previous values and the Mie coefficients a_v and b_v from the equations (40) & (41) into the cross-section scattering and extinction equations as in reference [30] we have:

$$C_{sca_v} = \frac{2\pi}{(K_v)^2} \sum_{l=1}^{l_{max}(0,G)} \left[(2l+1) \left[\left[\left| \frac{n_v \Psi(l, x_v) \psi(l, x_v n_v) - \psi(l, x_v) \Psi(l, x_v n_v)}{n_v \xi(l, x_v) \psi(l, x_v n_v) - \Psi(l, x_v n_v) \zeta(l, x_v)} \right|^2 \right] + \left[\left| \frac{n_v \Psi(l, x_v n_v) \psi(l, x_v) - \psi(l, x_v n_v) \Psi(l, x_v)}{n_v \Psi(l, x_v n_k) \zeta(l, x_v) - \psi(l, x_v n_k) \xi(l, x_v)} \right|^2 \right] \right] \right],$$

$$C_{ext_v} = \frac{2\pi}{(K_v)^2} \sum_{l=1}^{l_{max}(0,G)} \mathrm{Re} \left[(2l+1) \left[\left(\frac{n_v \Psi(l, x_v) \psi(l, x_v n_v) - \psi(l, x_v) \Psi(l, x_v n_v)}{n_v \xi(l, x_v) \psi(l, x_v n_v) - \Psi(l, x_v n_v) \zeta(l, x_v)} \right) + \left(\frac{n_v \Psi(l, x_v n_v) \psi(l, x_v) - \psi(l, x_v n_v) \Psi(l, x_v)}{n_v \Psi(l, x_v n_k) \zeta(l, x_v) - \psi(l, x_v n_k) \xi(l, x_v)} \right) \right] \right].$$

Finally placing our equations in a 2D graph we have:

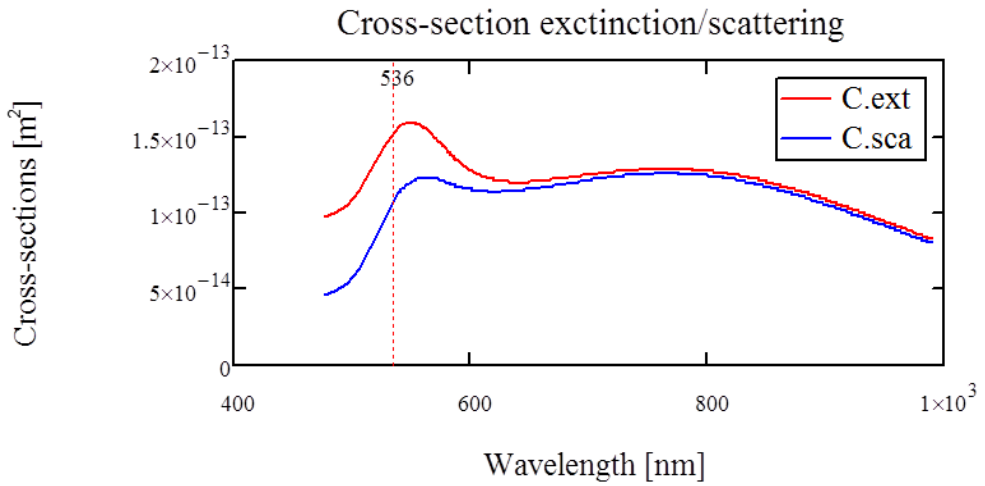

Fig. 24. Extinction and scattering cross-sections calculated for the gold nanoparticle with a size of 100 nm situated in water.

Note: If only one line is visible then the theoretical lines may be overlapped.

Non-exclusive license to reproduce thesis and make thesis public

I, Siim Heinsalu (date of birth: 01.21.1992),

1. herewith grant the University of Tartu a free permit (non-exclusive licence) to:

   1.1 reproduce, for the purpose of preservation and making available to the public, including for addition to the DSpace digital archives until expiry of the term of validity of the copyright, and

   1.2 make available to the public via the web environment of the University of Tartu, including via the DSpace digital archives until expiry of the term of validity of the copyright

Plasmon enhanced fluorescence in TiO_2:Sm^{3+} films doped by gilded nanoparticles,

(Title of thesis)

supervised by PhD Leonid Dolgov and PhD Ilmo Sildos,

(Supervisor's names)

2. I am aware of the fact that the author retains these rights.

3. I certify that granting the non-exclusive licence does not infringe the intellectual property rights or rights arising from the Personal Data Protection Act.

Tartu, 26.05.2014